RESEARCH ARTICLE

Sensitivity analysis and integrated optimization of placement and parameters of rotational friction dampers based on seismic energy approach considering soil-structure interaction

Hossein Jarrahi[1]*, **S. Javad Vaziri**[2], **Mohsen Khatibinia**[1]

1 Department of Civil Engineering, University of Birjand, Birjand, Iran, **2** Department of Civil Engineering, Semnan University, Semnan, Iran

* hossein.jarrahi@birjand.ac.ir

Abstract

The optimization of seismic resilience in steel moment-resisting frames (SMRFs) has driven extensive research into passive energy dissipation systems, particularly rotational friction dampers (RFDs). This study introduces a novel hybrid optimization framework that simultaneously determines the optimal placement and design parameters of RFDs in SMRFs. A sensitivity analysis of key RFD parameters, including frictional moment and rigid beam length, highlights their influence on seismic performance. The optimization problem is formulated based on the seismic energy dissipation concept, employing a modified binary and real-coded particle swarm optimization (BRPSO) algorithm. The study examines both 6- and 10-story SMRFs under artificial earthquake records, incorporating soil-structure interaction (SSI) effects to enhance accuracy. The results reveal that the optimal distribution of RFDs significantly reduces structural hysteretic energy and inter-story drift while improving energy dissipation efficiency. A comparative analysis shows that, for both SMRF configurations, an increase in the number of RFDs beyond the optimal threshold yields diminishing benefits in seismic mitigation. The proposed framework not only enhances structural resilience but also minimizes construction costs by ensuring an efficient damper layout. These findings provide valuable insights for designing cost-effective and high-performance seismic protection strategies for mid- to high-rise structures.

OPEN ACCESS

Citation: Jarrahi H, Vaziri SJ, Khatibinia M (2025) Sensitivity analysis and integrated optimization of placement and parameters of rotational friction dampers based on seismic energy approach considering soil-structure interaction. PLoS One 20(10): e0331741. https://doi.org/10.1371/journal.pone.0331741

Editor: Mohammadreza Vafaei, Universiti Teknologi Malaysia, MALAYSIA

Received: May 4, 2025

Accepted: August 20, 2025

Published: October 30, 2025

Copyright: © 2025 Jarrahi et al. This is an open access article distributed under the terms of the Creative Commons Attribution License, which permits unrestricted use, distribution, and reproduction in any medium, provided the original author and source are credited.

Data availability statement: Relevant data are available in Zenodo at https://doi.org/10.5281/zenodo.16989429.

Funding: The author(s) received no specific funding for this work.

1. Introduction

Recent advances in earthquake engineering focus not only on providing sufficient strength to structures but also on minimizing damage when they are subjected to seismic events [1–4]. The limited capacity of conventional seismic design codes to effectively dissipate seismic energy has driven the advancement and adoption of

Competing interests: The authors have declared that no competing interests exist.

passive control devices for both upgrading existing structures and designing new ones, aiming to enhance their seismic resilience, safety, and performance [5–9].

Tuned mass dampers (TMDs) are among the most extensively employed seismic energy dissipation devices utilized in the structural engineering domain to alleviate earthquake-induced forces in buildings and infrastructure. These devices, which function based on the principle of transferring vibrational energy to an auxiliary mass system, have long been recognized as effective passive control mechanisms for attenuating undesirable structural vibrations. Numerous studies have underscored the efficacy of TMDs in enhancing the dynamic performance of structures subjected to seismic excitation [10–15]. However, among these solutions, friction dampers stand out due to their exceptional energy dissipation efficiency and ease of integration into building systems. Their ability to minimize structural and non-structural damage during moderate to severe seismic events has been extensively validated through experimental research [16–25] Furthermore, friction dampers are particularly appealing due to their straightforward implementation, cost-effectiveness, and independence from external power sources, making them a reliable choice for passive structural control strategies [26–33]

The rotational friction damper (RFD), first introduced by Mualla and Belev [34], demonstrated significant potential in enhancing structural behavior against seismic forces, as evidenced by experimental and numerical analyses conducted on single-story frames. Subsequent research expanded on the applications of RFDs in enhancing seismic performance.

The innovative concept of the rotational friction damper (RFD), which was initially presented and discussed by the scholars Mualla and Belev in their seminal work [34], has shown remarkable promise in significantly improving the structural response and behavior of various architectural frameworks when subjected to the adverse effects of seismic forces, a fact that has been substantiated through a combination of both experimental and numerical analyses meticulously conducted on single-story frame structures. In the wake of these pioneering findings, subsequent scholarly research has broadened the scope of applications for RFDs, particularly in relation to their potential contributions to enhancing seismic performance across a diverse range of structural configurations. For example, the research conducted by Patel and Jangid [35] delved into the intricate seismic response characteristics of adjacent buildings that are interconnected via the strategic installation of RFDs, thereby offering valuable insights into their collective behavior during seismic events. In a similar vein, Kim and colleagues [36] undertook a comprehensive evaluation of the effectiveness of RFDs, rigorously assessing their capacity to improve the overall seismic response and behavior of various types of structural systems, thereby contributing to the foundational knowledge in this critical area of civil engineering. Furthermore, Kaur and colleagues [37] performed an in-depth analysis focused on the seismic performance of mid- to high-rise buildings that have been equipped with friction dampers, placing particular emphasis on their significant role in alleviating earthquake-induced deformations and forces that can compromise structural integrity and safety. Additionally, Choi and Kim [38] explored the integration of frictional hysteretic energy dissipation

mechanisms into reinforced concrete shear walls, which notably improved ductility under seismic loading. To address energy dissipation at low-frequency excitations, Sanati and colleagues [39] developed the rotational friction viscoelastic damper (RFVD), an enhanced RFD variant incorporating viscoelastic materials to improve energy dissipation under low-intensity vibrations. In order to assess seismic performance of buildings, Rayegani and colleagues [2] used four-joint RFDs (4J-RF) to enhance seismic resilience of buildings. The results of experimental and numerical analyses revealed that 4J-RF could efficiently dissipating energy and reducing residual displacements by up to 75%.

Subsequent advancements included Mirzabagheri et al.'s [40] research, which demonstrated that multi-unit RFD configurations achieved superior energy dissipation compared to single-unit systems. Bonchev and colleagues [41] introduced RFDs as seismic links for retrofitting SMRFs, effectively replacing traditional link elements to minimize damage during seismic events. Anoushehei and colleagues [42] conducted experimental studies to evaluate the cyclic performance of RFDs with different friction pad materials, providing insights into optimizing damper configurations. Furthermore, Nabid and colleagues [43] proposed a refined design methodology for friction wall dampers in RC frames to maximize energy dissipation efficiency. Extending this work, Nabid and colleagues [44] implemented a performance-based optimization framework for reinforced concrete frames equipped with friction dampers, achieving a more uniform distribution of damage across the building height by strategically adjusting the dampers' slip load. Collectively, these investigations highlight the RFD's versatility and reliability in enhancing seismic behavior across a diverse range of structural applications.

To effectively reduce seismic responses in structures, the design and optimal placement of passive dampers are critical [45,46]. Researchers have employed various methods to optimize damper configurations. Zhang and Soong [47] and Shukla and Datta [48] used sequential optimization for viscoelastic dampers in multi-story buildings. Moreschi and Singh [49] optimized friction dampers and metallic yielding elements simultaneously. Fallah and Honarparast [50] applied a genetic algorithm to optimize Pall dampers under two scenarios with uniform or unique slip loads. Miguel and colleagues [51] optimized the force and placement of friction dampers, while Kim and An [52] improved an existing building's seismic performance by optimizing damper distribution. In addition, self-centering systems have been identified as one of the innovative approaches utilized to mitigate lateral loads, such as those induced by earthquakes, in structural systems. A broad spectrum of previous studies has been dedicated to examining these so-called systems [53–55].

Jarrahi and colleagues [56] introduced an optimized design of RFDs by Utilizing a particle swarm optimization algorithm to enhance the seismic performance of inelastic SMRFs. Results indicate substantial reductions in roof displacement and hysteretic energy, confirming the RFD's efficacy under various earthquake records. In another study, they developed a hybrid optimization framework combining binary and real-coded particle swarm optimization to determine the optimal placement and parameters of RFDs in nonlinear SMRFs. By addressing energy dissipation efficiency and structural drift constraints, their study demonstrates that a strategically reduced number of RFDs can significantly mitigate seismic responses without imposing excessive costs [56]. Moreover, Jarrahi and colleagues [57] also evaluated SSI effects on the seismic performance of SMRFs equipped with optimal RFDs. In this study, optimizing the placement and parameters of RFDs for enhance seismic performance of SMRFs have been discussed. The outcomes highlighted the remarkable impact of SSI on energy dissipation and structural behavior under seismic loading.

During an earthquake, the base movement of a building differs from free-field ground motion due to soil deformations beneath the structure, influencing its seismic responses. The structural behavior is directly influenced by the underlying soil as a result of the interaction between the structure and the soil [58,59]. This phenomenon, known as SSI, becomes significant when the underlying soil is not very stiff or solid rock [60,61]. Structures on deformable soils exhibit seismic responses distinct from fixed-base assumptions commonly used in practice [62,63]. Traditionally, the effects of SSI have been considered advantageous [64,65]. However, recent studies have demonstrated that SSI can also produce detrimental impacts [66]. Consequently, incorporating SSI effects is crucial for accurate seismic evaluations.

Some prior investigations assessed the influence of SSI on buildings equipped with dampers. In this context Araz and Elias [67] optimized tuned mass dampers (TMDs) configurations for seismic vibration control, accounting for

SSI. Results demonstrate improved performance on soft soils, with reductions in displacements and accelerations under near and far-fault earthquakes. Also, the influence of key SSI parameters on the seismic efficiency of TMDs have been evaluated by Araz [68]. Numerical simulations on various building heights and soil conditions demonstrate that SSI significantly affects TMD performance, with reduced efficiency in low-rise structures on soft soils. Furthermore, soil nonlinearity effects on TMDs using a 3D FEM model have been analyzed by Wu and colleagues [69]. Results show that SSI reduces TMD effectiveness, especially in soft soils, while soil nonlinearity improves performance. Optimizing TMD parameters based on the soil-structure system frequency enhances seismic control compared to fixed-base design methods. Moreover, many other studies have analyzed SSI impacts on structural seismic behavior [70–74].

This investigation is primarily aimed at undertaking a comprehensive sensitivity analysis that pertains to the intricate design parameters associated with the yielding dampers, known as RFDs, which are specifically devised for the seismic protection SMRFs [75–77]. This study presents a novel contribution by conducting a comprehensive sensitivity analysis of the key parameters governing rotational friction dampers and enhancing their performance through parameter optimization, explicitly incorporating the influence of soil-structure interaction. Following this initial phase, the research proceeds to introduce a complex optimization problem that is fundamentally based on the seismic energy paradigm, with the objective of precisely determining the optimal configurations and specifications of the RFDs for both 6- and 10-story SMRFs when they are subjected to the dynamic forces generated by an artificial earthquake record. Within this analytical framework, the configuration of the RFDs, in conjunction with their frictional moment denoted as (M_f) and the length of their vertical rigid beam represented by (h_a), are meticulously identified as critical design variables, while the ratio that quantifies the maximum input energy relative to the maximum cumulative energy dissipated by the RFDs is systematically designated as the principal objective function of the optimization process. In order to effectively tackle the inherent challenges associated with this optimization task, a sophisticated hybrid methodology that integrates both binary and real-coded modified particle swarm optimization techniques, abbreviated as BRPSO, is employed to ensure a robust solution. Ultimately, the overall performance and efficacy of the SMRF that has been equipped with RFDs, which have been meticulously designed and optimized, is rigorously evaluated by incorporating the significant effects of soil-structure interaction (SSI) in response to four widely recognized real earthquake excitations, thereby facilitating a thorough understanding of the system's behavior under seismic loading conditions. This comprehensive approach not only enhances the resilience of the structures but also contributes valuable insights into the field of earthquake engineering, particularly in the domain of structural optimization. The findings of this research endeavor are anticipated to have profound implications for the future design and implementation of seismic protection systems within the context of modern engineering practices.

2. Rotational friction dampers

The various components that collectively constitute the system of RFDs, as illustrated comprehensively in Fig 1, encompass a pair of circular discs that are equipped with specialized friction pads, a unique central plate that is oriented vertically and positioned at the core, as well as two horizontal plates that extend laterally on either side. This intricate apparatus is meticulously attached to the central region of the beam via the aforementioned central plate, while the outermost boundaries of the lateral plates are firmly anchored to the supporting braces that provide stability. These braces are designed with the advanced capability of being pre-tensioned, a feature that is crucial in preventing any potential buckling phenomena when the structure is subjected to significant compressive forces that may arise during operational conditions. Thus, the effective interplay between these elements ensures the structural integrity and operational efficiency of the entire system under varying loads and stresses.

The frictional forces that are generated at the interface between the friction pads and the plates, when considered alongside the functionality of the bracing system, work in concert to effectively mitigate any potential movement of the

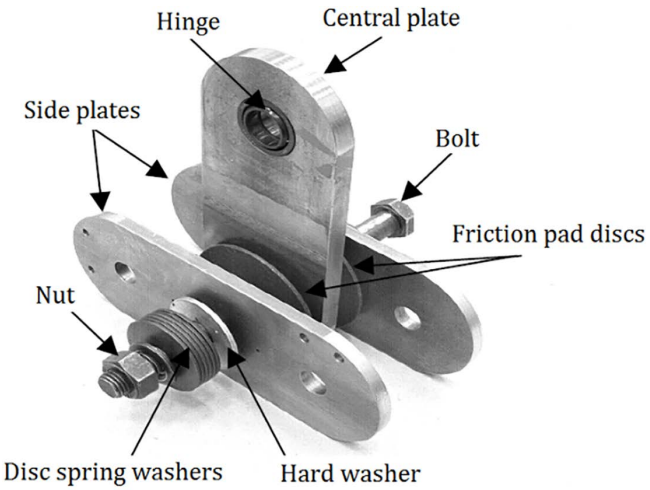


Fig 1. Specifications of the RFDs setup suggested by [34].

https://doi.org/10.1371/journal.pone.0331741.g001

frame during occurrences of seismic activity, thereby enhancing the overall stability and durability of the structure in question. Additionally, the operational dynamics of the RFDs are depicted in detail in Fig 2, which serves to highlight its remarkable capacity to dissipate energy efficiently, while simultaneously augmenting the seismic performance of the entire structural system, thereby ensuring greater resilience against the forces exerted during such events. Consequently, the integration of these mechanisms not only contributes to the immediate response of the structure under duress but also plays a pivotal role in the long-term sustainability and safety of the built environment in the face of unpredictable seismic occurrences.

The fundamental design parameters that are critical for the effective functionality of a RFD as well as its corresponding bracing system encompass several important elements, namely the frictional moment (M_f) which plays a pivotal role in the energy dissipation characteristics of the system, the pre-stressing force (F_p) that is meticulously applied to the bars to ensure adequate structural integrity and performance under various loading conditions, the cross-sectional area (A_b) of the bars which directly influences the load-bearing capacity and overall stiffness of the damper system, and lastly, the dimensions pertaining to the length of both the central and side rigid plates (h_a) which are essential in determining the overall geometric configuration and effectiveness of the bracing system in mitigating dynamic forces during seismic events. The detailed design principles and methodologies of the RFD have been thoroughly studied by Nielsen and Mualla [78]. Additionally, the relationships and equations governing the design process are comprehensively presented in Mualla [79], providing essential insights for the effective application of this damping system.

3. Sensitivity analysis

In this section, the model described in the Mualla [34] article in the previous part is subjected to sensitivity analysis, and the influence of parameters M_f, F_p, h_a, and r on system behavior is studied. Initially, the parameters h_a (length of the vertical plate of the damper) and "r" (half the length of the horizontal plate of the damper) are considered as variables. The values of h_a are selected from 0.1, 0.2, 0.3, 0.4, and 0.5, while the values of "r" are chosen from 0.0826, 0.1652, 0.2478, 0.3304, and 0.4130. It is evident that the matrix formed by h_a and "r" constitutes a 5×5 matrix, where the diagonal elements represent the concentric installation configuration, and the remaining elements denote the eccentric installation configuration. For instance, when $h_a = 0.4$ and $r = 0.3304$, the system is concentric; for other possible values of r, the system becomes eccentric. It is noteworthy that a concentric system is defined as one where the intersection of the brace

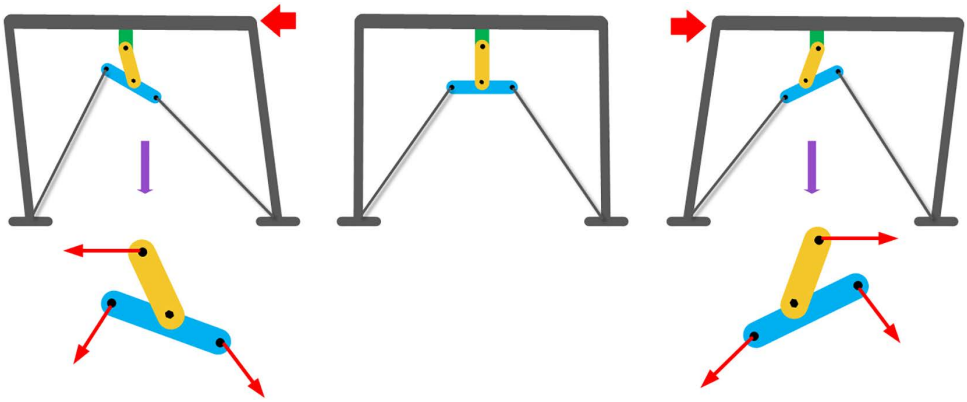


Fig 2. The RFD's behavior mechanism (2002).

https://doi.org/10.1371/journal.pone.0331741.g002

axes passes through the connection point of the damper and frame beam. Conversely, when this intersection occurs above or below the damper-beam connection point, the system is classified as eccentric [78].

Figs 3–5 illustrate, respectively, the effect of damper geometry (h_a and r) on the energy dissipation of the damper (ED), the maximum horizontal displacement of the frame (MaxDisp), and the stiffness of the damper and braces system (K). All units in these figures are expressed in kgf-m.

Based on Fig 3, it is evident that the maximum energy dissipation occurs in the concentric installation configuration. Moreover, increasing the length of the damper plates enhances the dissipated energy. Also, the minimum horizontal displacement of the frame is achieved in the concentric installation configuration, as shown in Fig 4. Notably, the least

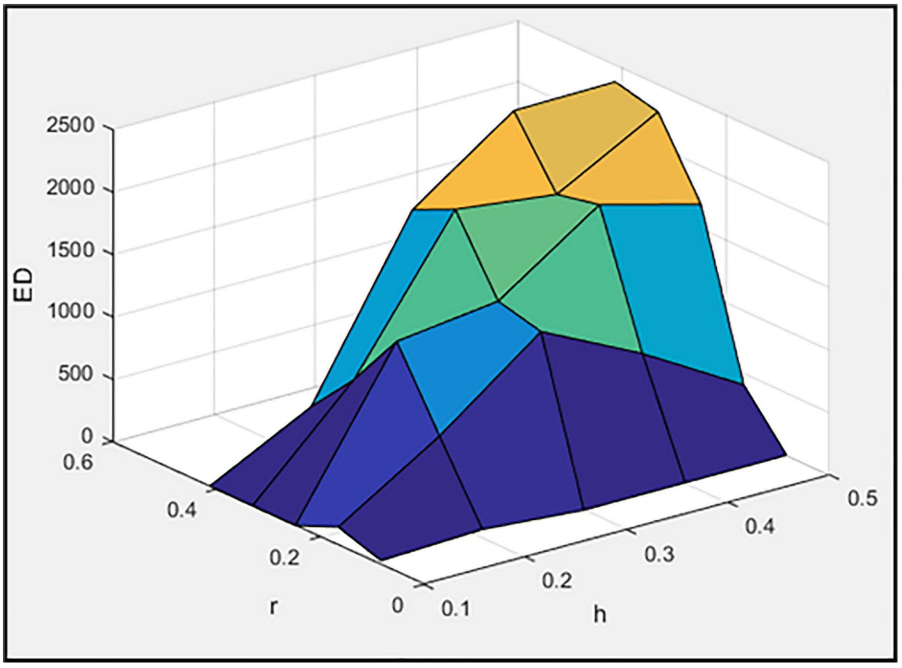


Fig 3. The effect of h_a and r values on dissipated energy.

https://doi.org/10.1371/journal.pone.0331741.g003

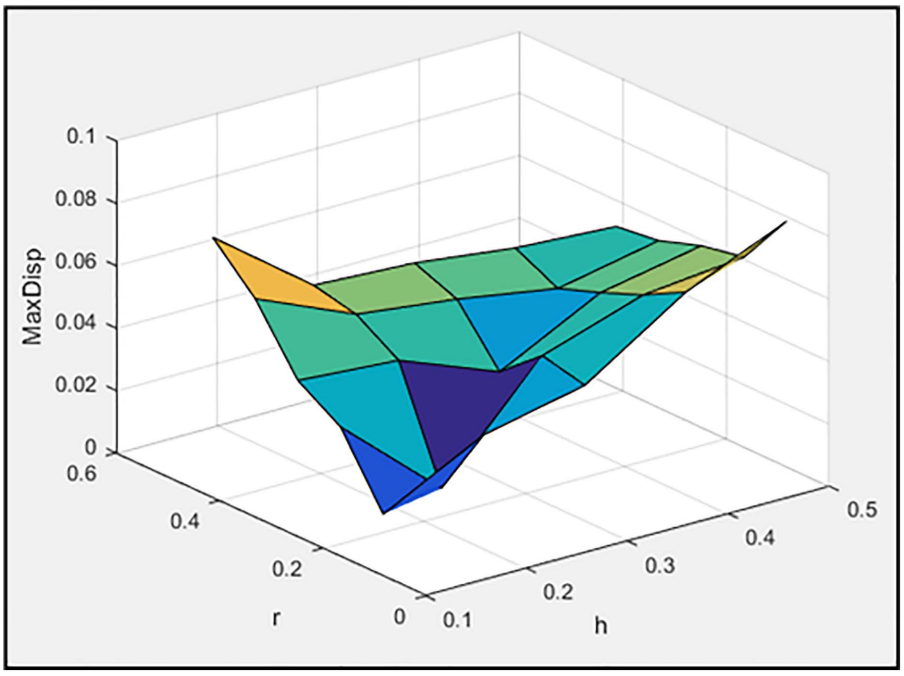


Fig 4. The effect of h_a and r values on maximum displacement of frame.

https://doi.org/10.1371/journal.pone.0331741.g004

displacement is observed at h_a = 0.2 and r = 0.1652, values that are neither the maximum nor minimum of their respective ranges. Consequently, it cannot be stated as a general rule that increasing or decreasing these two parameters will always reduce the maximum frame displacement. Instead, an optimal range for these parameters must be identified. Moreover, Fig 5 clearly demonstrates that the concentric installation configuration results in the highest stiffness for the damper and braces system. Additionally, increasing the length of the damper plates leads to an increase in system stiffness. As mentioned in the introduction, the governing parameters (including stiffness) for moment frames with chevron braces equipped with these dampers can be found in reference [78].

In the second stage, h_a and r are set to 0.2 and 0.1652, respectively, while the parameters M_f (slip friction moment) and F_p (pre-tension force of the braces) are considered as variables. The values of M_f are selected from 2000, 3,000, 4,000, 5,000, and 6,000, while the values of F_p are defined as six times the corresponding M_f values. Figs 6–8 illustrate the effects of M_f and F_p on the energy dissipation of the damper (ED), the maximum horizontal displacement of the frame (MaxDisp), and the stiffness of the damper and braces system (K), respectively. All units in these figures are expressed in kgf-m. Fig 6 clearly demonstrates a pronounced inverse relationship between the slip friction moment and the amount of energy dissipated (ED). As M_f increases, the system's ability to dissipate energy diminishes markedly. This is primarily due to the fact that a higher slip friction moment restricts the damper from transitioning into its sliding phase, which is essential for energy dissipation through friction. Conversely, F_p appears to exert only a marginal influence on energy dissipation, suggesting that it is not a primary controlling parameter in this context. Fig 7 presents the variation of the maximum displacement of the frame with respect to M_f and F_p. Although there are slight changes in displacement values with increasing M_f and F_p, the overall trend remains relatively flat. This implies that neither parameter has a substantial impact on frame displacement, which could be attributed to the fact that displacement is more sensitive to system-level dynamics rather than isolated damping or bracing characteristics. Fig 8 sheds light on the influence of M_f and F_p on the stiffness of the damper-brace system (K). As illustrated, variations in these parameters do yield

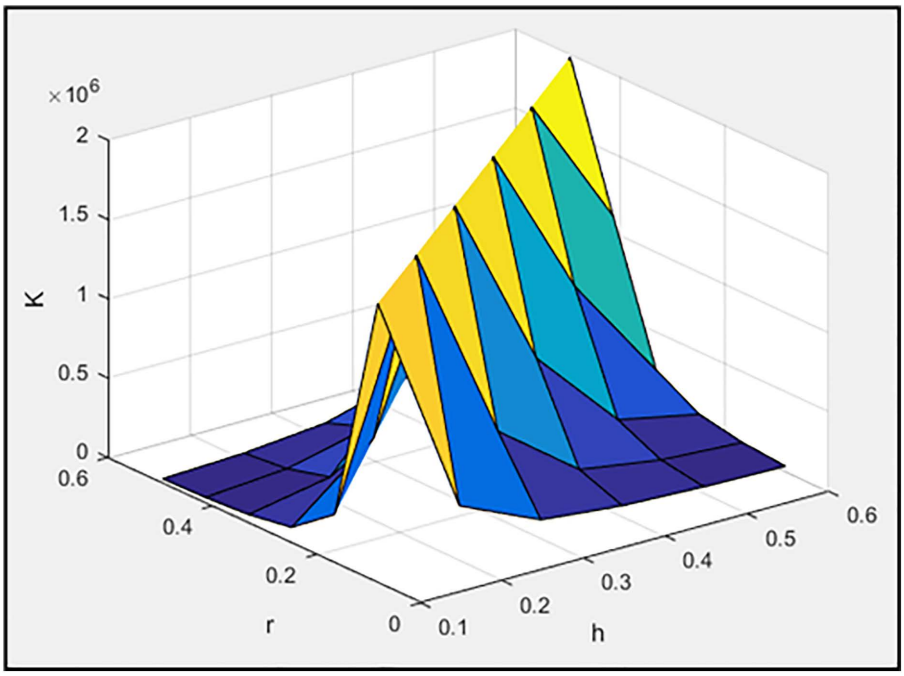


Fig 5. The effect of h_a and r values on the stiffness of the damper and brace system.

https://doi.org/10.1371/journal.pone.0331741.g005

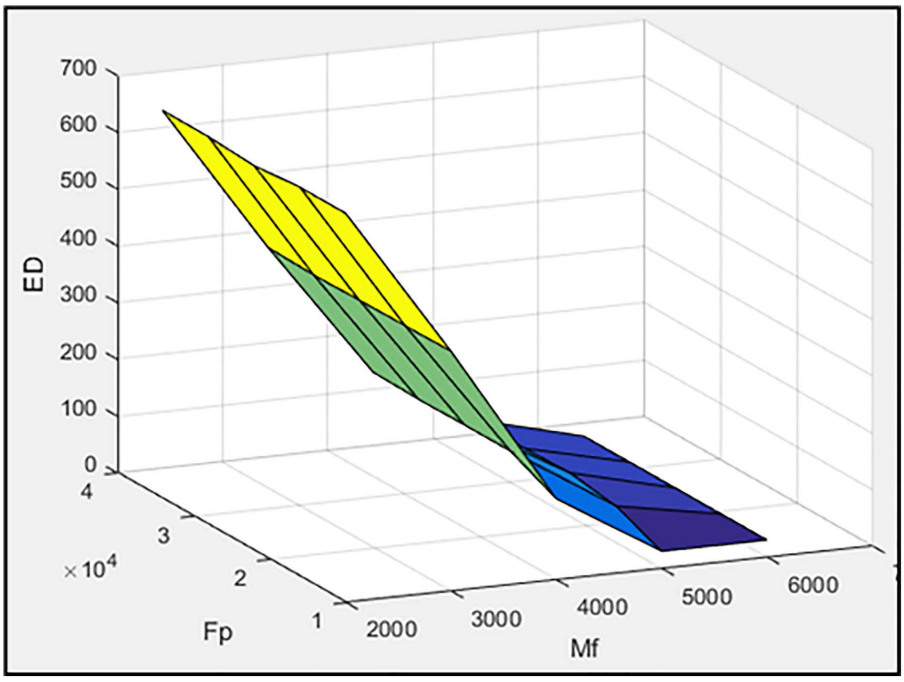


Fig 6. The effect of M_f and F_p values on dissipated energy.

https://doi.org/10.1371/journal.pone.0331741.g006

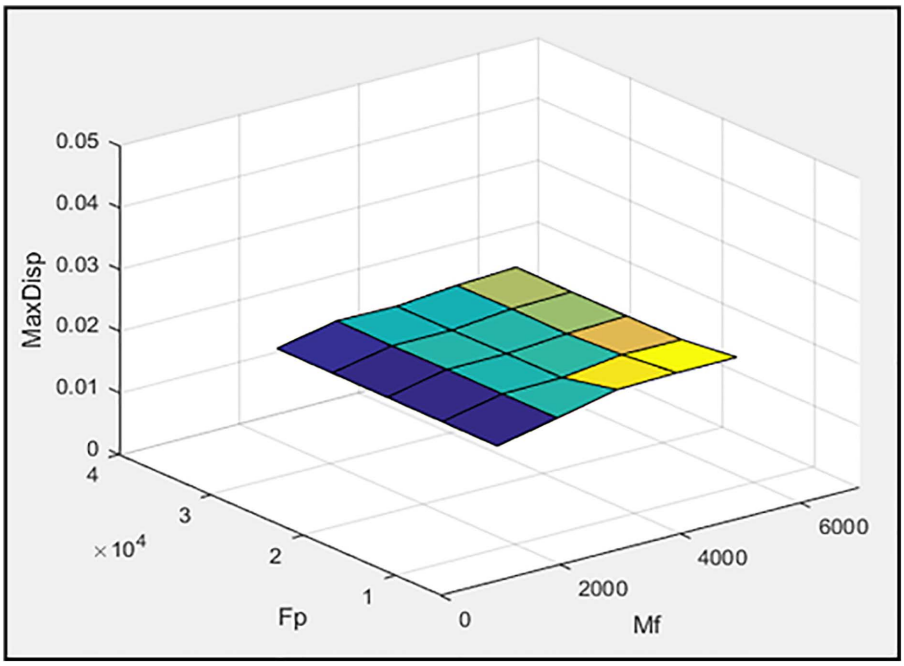


Fig 7. The effect of M_f and F_p values on maximum displacement of frame.

https://doi.org/10.1371/journal.pone.0331741.g007

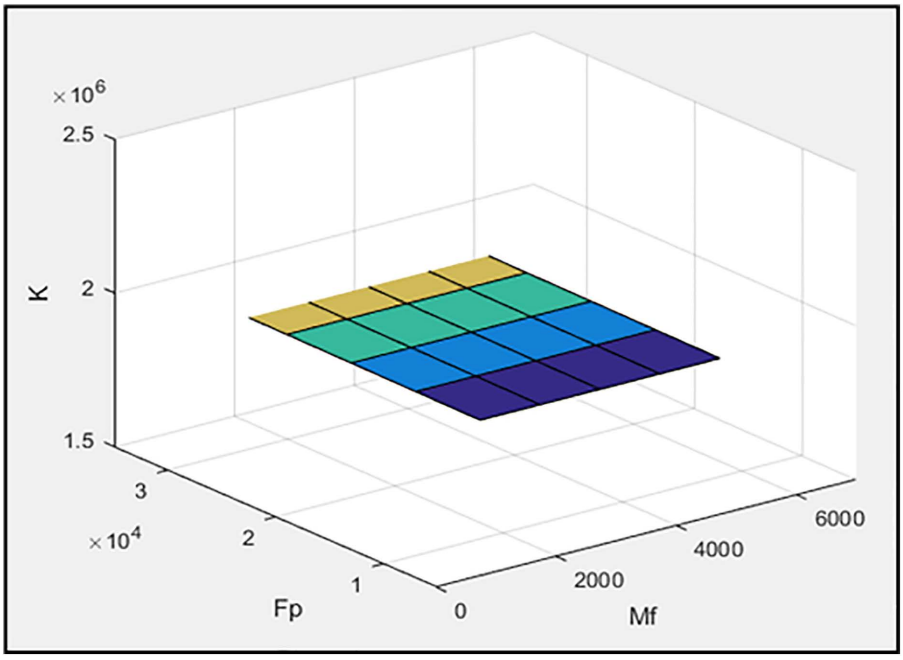


Fig 8. The effect of M_f and F_p values on the stiffness of the damper and brace system.

https://doi.org/10.1371/journal.pone.0331741.g008

slight modifications in the overall stiffness. However, much like in the case of displacement, the observed changes are not significant. This again indicates that the system's stiffness is relatively robust against moderate changes in either slip moment or pre-tension force.

4. Seismic energy approach

The ability of a structural system to withstand seismic events is contingent on its capacity to dissipate seismic energy through various mechanisms, including kinetic energy, damping energy, inelastic hysteresis, and elastic strain energy [80–84]. The incorporation of RFDs enhances this dissipation through frictional mechanisms, thereby improving the system's overall energy absorption efficiency. The governing equations describing structural motion and energy distribution have been extensively explored in previous studies [56,57,85]. In the present work, the methodology previously developed is employed to quantify input energy, cumulative hysteretic energy, and dissipated energy within RFD-integrated systems. The energy balance equation and associated formulations for kinetic, damping, and absorbed energy remain consistent with prior research, with additional refinements tailored to the specific characteristics of the current study.

5. Particle swarm optimization algorithm

Metaheuristic optimization algorithms have been widely utilized in structural optimization [86–95], with Particle Swarm Optimization (PSO) being a prominent example due to its adaptability to both continuous and discrete variables. Although the convergence speed of PSO is very slow towards the global optimum and is trapped by poor local minima. Hence, diverse variants of PSO algorithm were developed for overcoming its drawbacks.

Originally inspired by the coordinated movements of bird flocks, PSO iteratively refines candidate solutions until convergence criteria are met. The Real-Coded PSO (RPSO) and Binary-Coded PSO (BPSO) variants offer tailored approaches for different problem formulations, utilizing velocity and position updates to navigate the solution space. To enhance convergence and mitigate local optima entrapment, Modified PSO (MPSO) incorporates an additional stochastic perturbation factor. The mathematical foundations and implementation details of these algorithms have been extensively addressed in prior studies [56,57], forming the basis for their application in the present research.

6. Modeling assumptions

6.1. Modeling of RFD

The intricacies involved in the modeling processes and the subsequent verification of the RFD within the computational framework of OpenSees are thoroughly elucidated in the present section. The distinctive behavior of the frictional hinge was meticulously simulated through the implementation of a zero-length element that exhibited an elastic-perfectly plastic response, characterized by an exceptionally high initial stiffness that is critical for accurate modeling. In order to facilitate this simulation, two nodes possessing identical spatial coordinates were strategically defined at the location of the frictional hinge, and their translational degrees of freedom were effectively constrained to ensure proper functionality. The bracing bars, fundamental components of the structural system, were adeptly modeled utilizing the corotTruss element, which allows for the capture of the non-linear behavior associated with such elements. Furthermore, the pre-tensioned force present in the bracing bars was integrated into the model through the initial strain technique, which was operationalized via the innovative use of InitStrainMaterial, thus ensuring that the behavior of the bars under load was accurately represented. To substantiate the efficacy of the RFD modeling approach employed in OpenSees, a rigorous validation process was undertaken, wherein an elastic single-story SMRF that was equipped with an RFD, previously investigated by Mualla and Belev [34], was meticulously considered within the broader scope of the study conducted by Jarrahi et al. [56,57,96]. This comprehensive validation was essential to ensure that the modeling techniques accurately reflected the physical behavior of the system under various loading conditions. The careful attention to detail in modeling components

such as the frictional hinge and the bracing bars serves to enhance the reliability of the computational results, thereby contributing to a more profound understanding of the RFD's impact on structural performance.

6.2. Modeling of an SMRF

The computational analyses conducted in this research are carried out on 6- and 10-story SMRF, which were established as a reference structure by Wong [97] and subsequently by Wong and Johnson [98]. The characteristics of the structural framework are depicted in Fig 9.

The total mass associated with each individual story, along with the uniformly distributed load acting upon the beams of the 6-story SMRF, was meticulously assumed to be a significant value of 2,942 kN, while the uniformly distributed load was designated to be 21.89 kN/m, thereby establishing a foundational parameter for the structural analysis. In a parallel manner, when considering the 10-story SMRF, these crucial parameters were respectively taken as a total mass of 2,147 kN and a uniformly distributed load of 21.89 kN/m, ensuring consistency across the modeling framework. Furthermore, a damping ratio of 3% was uniformly adopted for both structural models, reflecting a common practice in structural dynamics to account for energy dissipation mechanisms. In addition, the yield stress (Fy) of the structural steel was precisely defined at a value of 248.2 megapascals (MPa), while the modulus of elasticity (E) for the steel was established at a value of 2×10^5 megapascals (MPa), which are both critical parameters in determining the material behavior under various loading conditions. The lumped plasticity model was effectively implemented within the analysis framework by utilizing zero-length plastic hinges strategically located at the ends of the elastic beam-column elements, as meticulously illustrated in the accompanying Fig 10. To accurately capture the bilinear hysteretic response characteristic of these structural elements, the Ibarra–Medina–Krawinkler (IMK) model [100] was employed, with its pertinent properties comprehensively depicted in Fig 11 for further clarity. It is important to note that both aforementioned frames have undergone rigorous validation in prior research conducted by Jarrahi and colleagues, as referenced in studies [56,57,85].

6.3. Soil-structure interaction (SSI) modeling procedure

SSI plays a critical role in influencing structural behavior, especially in buildings equipped with damping systems [102]. In this study, SSI was modeled using the direct finite element approach developed by Jaya and Prasad [103]. This method enables the simultaneous modeling of both the soil and structural components, thereby facilitating a detailed assessment of their nonlinear dynamic behavior using OpenSees simulations. The finite element configuration of the SSI system is depicted in Fig 12.

Rayhani and Naggar [104] experimentally examined the impact of varying horizontal soil boundary distances on the seismic response of different structural systems. Their analysis considered two boundary distances, 10B and 5B, where *B* denotes the foundation width. The results revealed that increasing the boundary distance from 5B to 10B produced only a marginal 5% change in seismic response, while significantly reducing computational cost and processing time. Furthermore, their findings confirmed that seismic wave amplification is primarily concentrated within the upper 30 meters of the soil profile, consistent with contemporary seismic design codes, which base local site effect assessments on the properties of the top 30 meters of soil. Based on these observations, the current study adopted a horizontal soil boundary distance of five times the structure's width (4,500 inches) and assumed a soil domain depth of 30 meters. The soil domain was modeled using isoparametric four-node quadrilateral elements under plane strain conditions, with a constant out-of-plane thickness equivalent to the inter-frame spacing. Fig 13 presents the modified pressure-independent multi-yield J2 plasticity model introduced by Zhang and colleagues [105], with parameters calibrated according to the guidelines specified in the OpenSees manual.

To simulate radiation damping and prevent the artificial reflection of outward-propagating shear and dilatational waves, Lysmer–Kuhlemeyer dashpots, originally proposed by Lysmer and Kuhlemeyer [106], were applied at the free-field boundaries of the soil domain. These dashpots, illustrated in Fig 12, function by absorbing seismic energy at the model

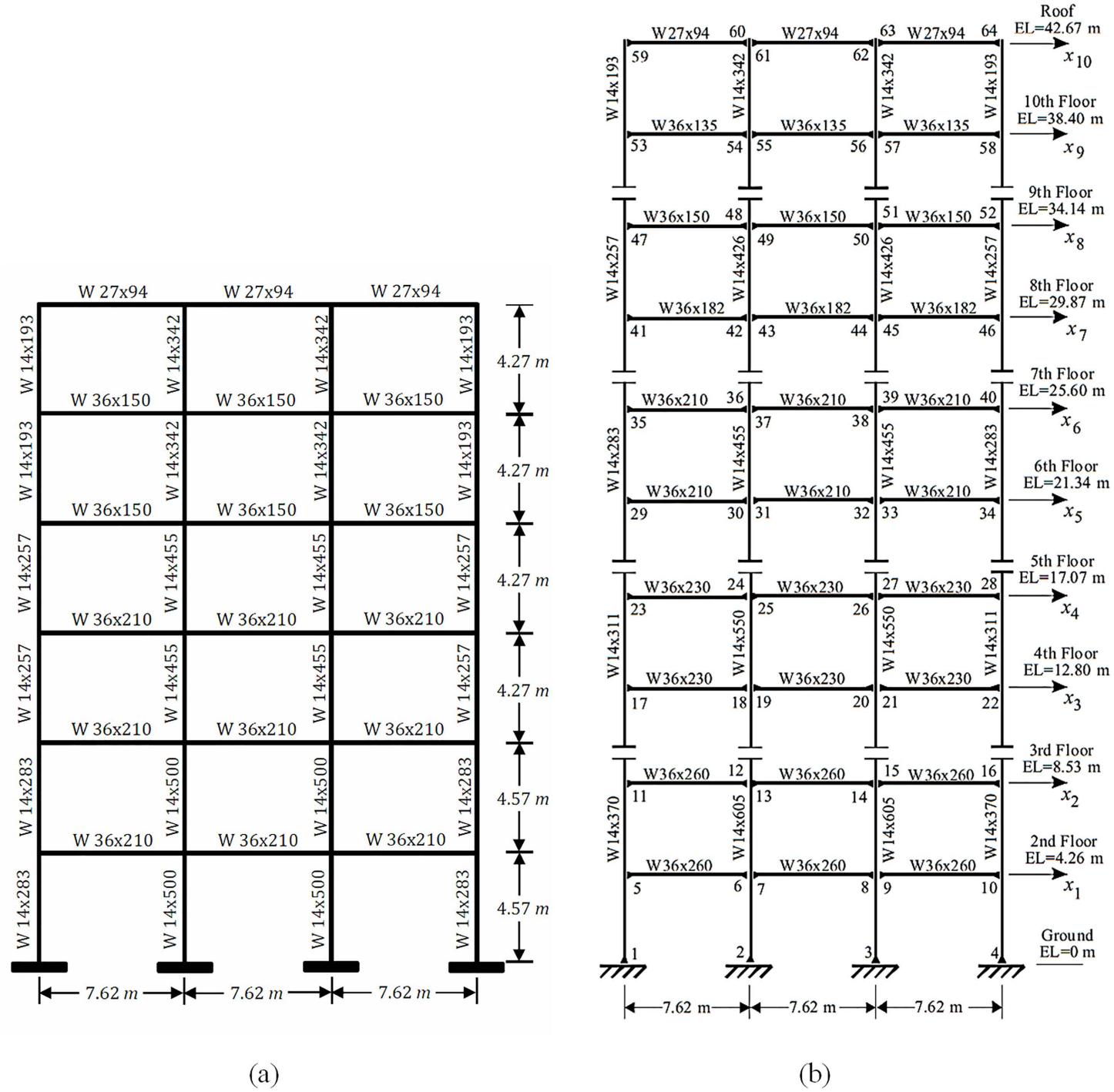


Fig 9. Characteristic of 6- and 10-story SMRF [99,98].

https://doi.org/10.1371/journal.pone.0331741.g009

boundaries. In this study, the dashpots were implemented using zero-length elements assigned with a viscous uniaxial material model. For a comprehensive explanation of their formulation and mechanical behavior, readers are referred to Lysmer and Kuhlemeyer [106]. The raft foundation was idealized as rigid, and the interface between the foundation and

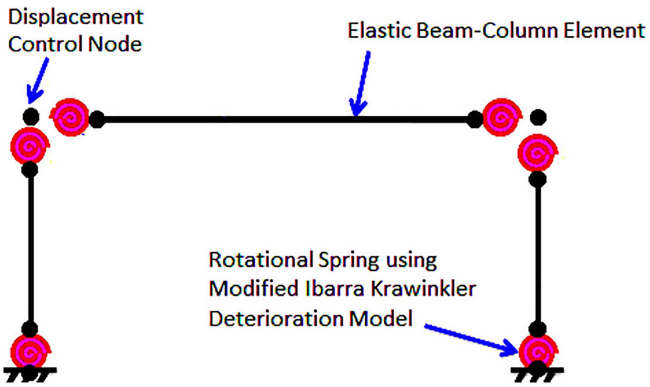


Fig 10. The SMRF characterized by lumped plasticity within the OpenSees.

https://doi.org/10.1371/journal.pone.0331741.g010

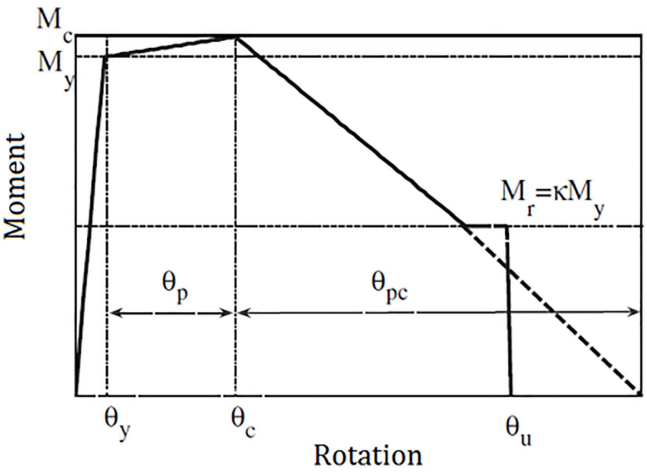


Fig 11. The monotonic response curve of the modified IMK [100,101].

https://doi.org/10.1371/journal.pone.0331741.g011

the surrounding soil was modeled using nodes with appropriate constraints. To ensure compatible displacement between the soil and foundation in both horizontal and vertical directions, the *equalDOF* command was employed in the X and Y directions. The primary soil material properties used in the numerical simulations are listed in Table 1, while supplementary parameters were derived from shear wave velocity (Vs) and Poisson's ratio (ν), following the guidelines provided by Khatibinia and colleagues [73].

7. Optimization of placement and parameters of RFDs for seismic protection of SMRF

This section meticulously delineates the concurrent optimization processes that are employed in the strategic placement as well as the intricate design parameters of RFDs, which are specifically intended for the enhancement of seismic protection measures applicable to SMRFs.

7.1. Problem optimization

In this context, the location vector of the RFDs (P) is characterized as an N_p-dimensional binary vector, wherein each component assumes a value of either 1 or 0, signifying the existence or non-existence of a damper, respectively. Considering

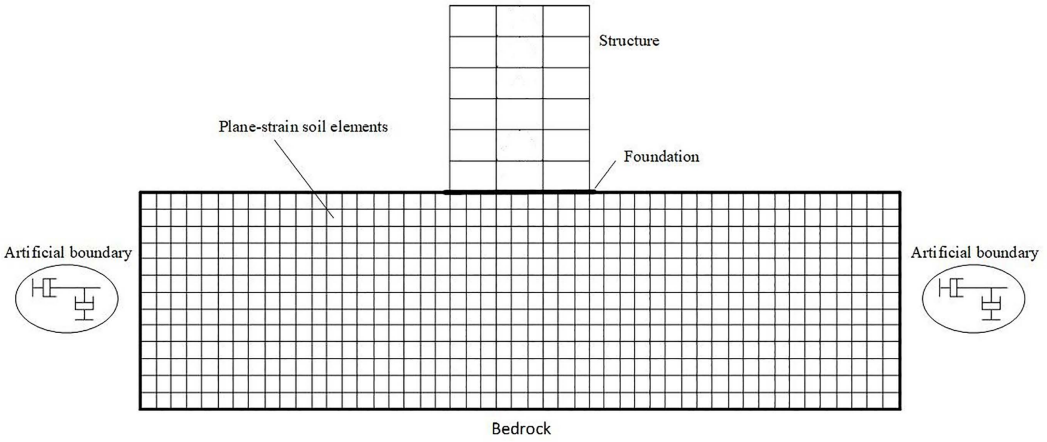


Fig 12. Fithe fnite element modeling framework developed for the SSI system, implemented using the OpenSees simulation platform.

https://doi.org/10.1371/journal.pone.0331741.g012

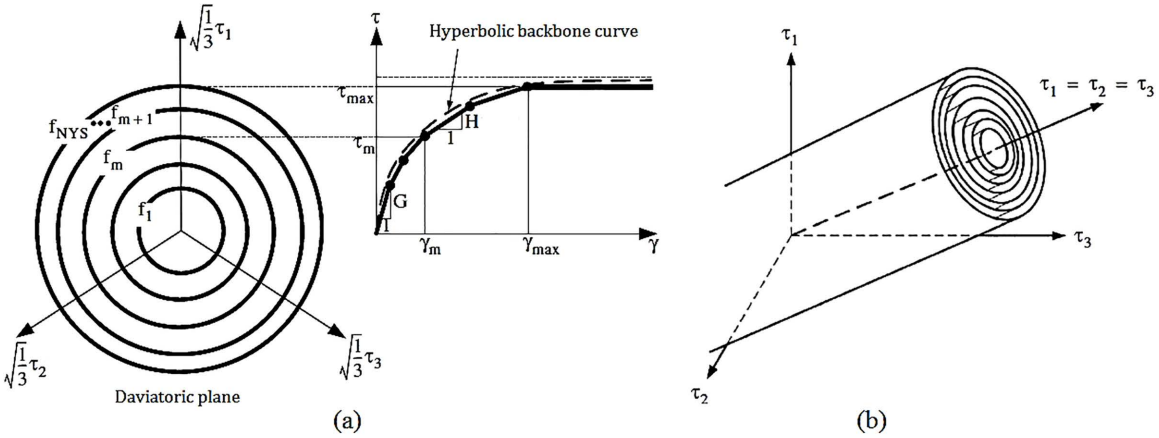


Fig 13. Illustration of the multi-yield-surface formulation based on the J2 plasticity theory: (a) Octahedral representation of shear stress–strain response; (b) multi-surface Von Mises yield criteria [105].

https://doi.org/10.1371/journal.pone.0331741.g013

Table 1. Summary of the governing parameters and constitutive criteria adopted in the development of the pressure-insensitive multi-yield plasticity formulation.

Parameter	Description	Value
$V_s\,(\mathrm{m/s})$	Shear wave velocity	275
$\rho\,(\mathrm{ton/m^3})$	Mass density	1.7
v	Poisson's ratio of soil	0.35
ϕ	Friction angle at peak shear strength	24
ζ	viscous damping	10%

https://doi.org/10.1371/journal.pone.0331741.t001

that the upper limit of dampers that can be integrated into the SMRF is represented by N_d, the vector P delineates the various potential configurations for damper placement within the structure. For the N_d dampers, a design vector that encompasses the frictional moment (M_f) and the vertical rigid beam length (h_a) is proposed, with both being regarded as

continuous design variables. Consequently, all design variables are aggregated into a (N_p + N_d × 2)-dimensional vector (i.e., X = {P, M_f, h_a}). The optimization challenge is constrained by a limit on the maximum inter-story drift of the structure. The objective function is articulated as the maximum seismic input energy (E_i) that penetrates the structure, normalized by the maximum cumulative energy dissipated within the RFDs (E_{RFDs}). Thus, the concurrent optimization of RFD distribution and design parameters can be articulated as follows:

$$\begin{aligned} &\text{Find}: \quad X = \{P, M_f, h_a\} \\ &\text{Minimize}: f(\boldsymbol{X}) = \frac{E_i(\boldsymbol{X})}{E_{RFDs}(\boldsymbol{X})} \\ &\text{subject to}: \delta(\boldsymbol{X}) \le \delta_{all} \\ &\qquad h^i_{a,\min} \le h^i_a \le h^i_{a,\max},\ i = 1, 2, ..., N_d \\ &\qquad M^i_{f,\min} \le M^i_f \le M^i_{f,\max},\ i = 1, 2, ..., N_d \end{aligned} \tag{1}$$

where $h^i_{a,min}$ and $h^i_{a,max}$ denote the lower and upper limits of the vertical rigid beam length associated with the ith damper, respectively; $M^i_{f,min}$ and $M^i_{f,max}$ represent the lower and upper limits of the frictional moment attributed to the ith damper, respectively. is the permissible threshold of the inter-story drift. In order to integrate constraints within the optimization framework, Coello [107] undertook an extensive investigation into techniques for handling constraints. Notably, the external penalty function has emerged as one of the most prevalently utilized methodologies in structural optimization [108–110]. By employing this strategy, the constrained optimization challenge associated with the RFD can be reformulated into an unconstrained format. This technique articulates the penalized objective function in the following manner:

$$\widetilde{f}(X) = f(X)\,(1 + r_p P_f) \tag{2}$$

where P_f is the total penalty; and r_p is an adjusting coefficient introduced by Chen and Chen [108] as:

$$r_p = r_{p1}\,[1 + 0.2(l - 1)] \le 4 r_{p1} \tag{3}$$

where r_{p1} is an initial adjusting value in the first iteration and l is the generation counter. It is noted that the selection reason of penalty coefficient and their sensitivity to optimization performance have been discussed in the previous studies such as Rajeev and Krishnamoorthy [111].

7.2. *Optimization of placement and parameters* of *RFDs*

In the context of this research, a novel hybrid optimization algorithm has been meticulously crafted, which integrates both binary and real-coded modified Particle Swarm Optimization (PSO) techniques. This innovative approach, which has been designated as BRPSO, has been specifically designed to concurrently optimize not only the strategic placement but also the critical parameters of the RFDs utilized within the framework of the 6- and 10-story SMRF depicted in Fig 9. To facilitate this intricate optimization process, the maximum permissible quantity of RFDs that can be incorporated into the structural design has been formally denoted by the symbol N_d. In pursuit of ascertaining the most advantageous placement of the RFDs, each particle within the BRPSO algorithm has been assigned a binary string, referred to as P, which comprises a total of N_p bits. It is noteworthy that, in this specific formulation, N_p has been established as 10, which directly correlates to the total number of stories present within the structural configuration being analyzed. Within this binary representation system, a value of 1 located at the i-th position of the binary string P unequivocally indicates the presence of an RFD positioned at the i-th story level, while conversely, a value of 0 signifies the complete absence of an RFD at that particular elevation. Progressing to the subsequent phase of the optimization process, a N_d × 2-dimensional vector has been assigned to each particle, which serves the purpose of encapsulating the essential parameters associated with the RFDs that have been installed. It is crucial to emphasize that these specific parameters are exclusively linked to the positions within the

binary string P where the value has been identified as 1, thus ensuring a direct correlation between the binary representation and the physical attributes of the dampers. The comprehensive optimization procedures, alongside the intricate encoding strategy employed within the BRPSO framework, are visually represented and elucidated in detail within Fig 14, thereby providing a clearer understanding of the methodological advancements achieved through this research initiative.

8. Numerical results of optimization

The most advantageous arrangement of RFDs, in conjunction with the associated parameter values that correspond to these distributions, was meticulously executed for frames characterized by 6- and 10-stories in the context of SMRFs. In addition, the established upper and lower bounds concerning the design variables that are relevant to the RFDs are comprehensively detailed and presented in Table 2, which serves as a critical reference point for understanding the constraints and limits imposed on the design process.

In the present research, the parameter values for the RBPSO were established in accordance with the comprehensive guidelines outlined by Gharehbaghi and Khatibinia [87]. Consequently, the upper limit for the number of iterations (Imax) and the size of the population (N) were designated as 100 and 30, respectively. The minimum and maximum weight coefficients (i.e. ωmin and ωmax) and were allocated values of 0.1, 0.4, and 25, correspondingly. Moreover, the optimal configuration for the RFDs along with their associated parameter values were initially computed for the SMRF subjected to a simulated earthquake event. The synthetic seismic record was generated utilizing the well-established Kanai–Tajimi methodology. This technique conceptualizes seismic excitation as a stationary process, wherein the input motion is depicted as a white noise signal. The power spectral density (PSD) function of the excitation is articulated as follows:

$$S_{K.T}(\omega) = S_0 \left[\frac{{\omega_g}^4 + 4{\zeta_g}^2{\omega_g}^2\omega^2}{(\omega^2 - {\omega_g}^2)^2 + 4{\zeta_g}^2{\omega_g}^2\omega^2} \right]; S_0 = \frac{0.03\zeta_g}{\pi\omega_g(4{\zeta_g}^2 + 1)} \tag{4}$$

where S_0 denotes the invariant spectral density. Furthermore, the frequency and the fundamental damping coefficient are postulated to be 25.13 rad/s (equivalent to 4 Hz) and 0.8, respectively, in accordance with the findings of Wu and colleagues [112] for Site Class C, as delineated in ASCE 7-16 [64]. The PGA of the synthetically generated earthquake employed in the optimization procedure was established at 0.7g for the 6-story framework and 0.4g for the 10-story configuration. Additionally, Fig 15(a) and (b) depict the temporal progression of the aforementioned synthetic seismic records.

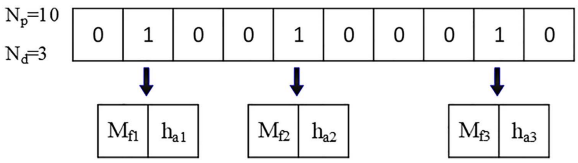


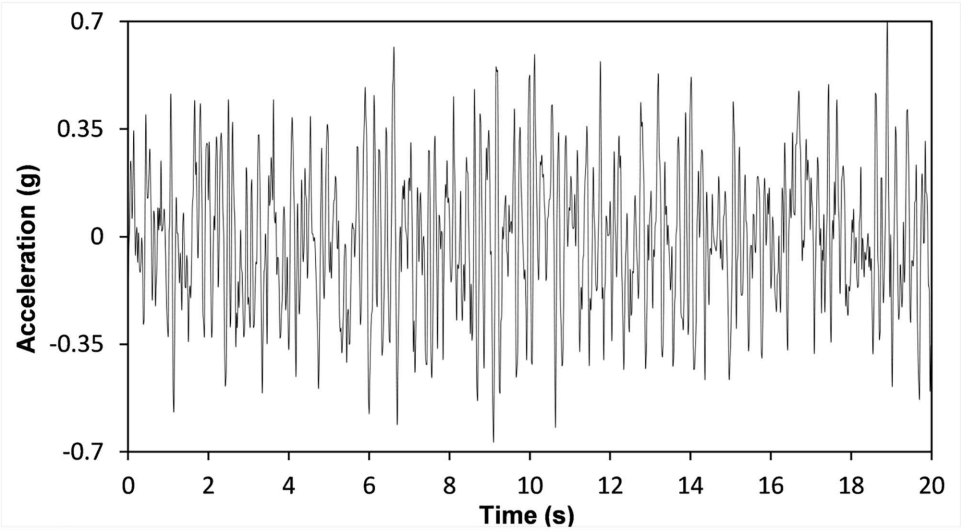
Fig 14. the functioning of BRPSO.

https://doi.org/10.1371/journal.pone.0331741.g014

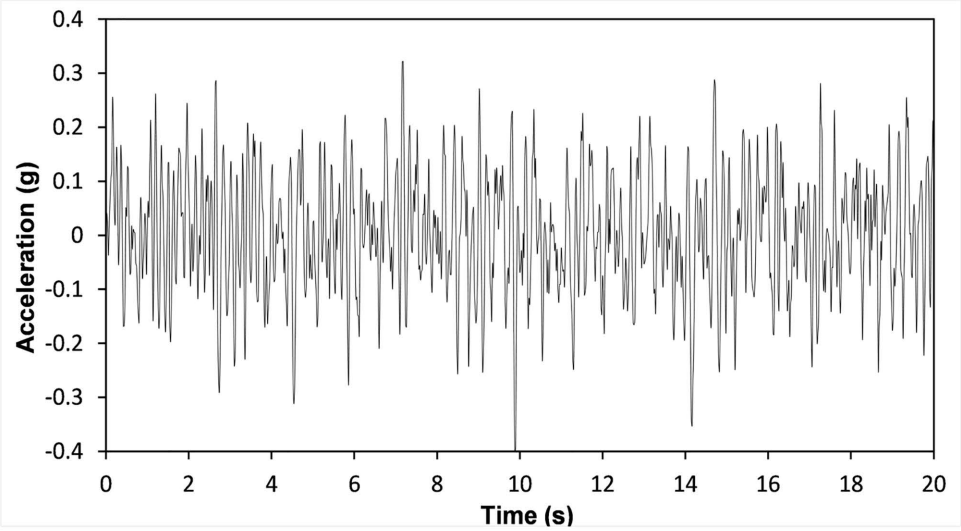
Table 2. Defined Ranges for RFD Parameter Values in 6- and 10-Story SMRFs.

RFD parameter	SMRF	Lower bound	Upper bound
M_f (Kips.in)	6-Story	200	3,000
	10-Story	300	4,000
h_a (in)	6-Story	5	25
	10-Story	5	25

https://doi.org/10.1371/journal.pone.0331741.t002



(a)



(b)

Fig 15. Time history of artificial record with a PGA of (a) 0.7g and (b) 0.4g.

https://doi.org/10.1371/journal.pone.0331741.g015

A total of five separate optimization executions were conducted, resulting in the identification of the optimal solution that produced the minimum value for the objective function, which was recognized as the global optimum for the RFDs. This study examined and determined the ideal configuration of the RFDs along with their associated parameter values for varying N_d in both 6- and 10-story structural frameworks. The optimal arrangement of the dampers, along with the corresponding values of the objective function, is presented in Table 3.

The optimization outcomes delineated in Table 3 indicate that an augmentation in the optimal RFDs within the SMRF framework leads to a reduction in the objective function. A comparative analysis of the objective function values demonstrates that a negligible difference is noted when the quantity of RFDs is increased from 5 to 6 for a 6-story frame.

Table 3. Optimal Damper Configurations and their Associated Objective Function Values.

Nd	6-Story		10-Story	
	Best placement	**Objective function**	**Best placement**	**Objective function**
1	[0,0,0,0,0,1]	2.185	[0,0,0,0,0,0,0,0,0,1]	4.767
2	[0,0,0,0,1,1]	1.952	[0,0,0,0,0,0,0,0,1,1]	3.834
3	[1,0,0,1,0,1]	1.702	[1,0,0,0,0,0,1,0,0,1]	2.993
4	[1,0,0,1,1,1]	1.406	[1,0,0,1,0,1,0,0,0,1]	2.416
5	[1,0,1,1,1,1]	1.194	[1,0,0,1,0,1,0,1,0,1]	2.053
6	[1,1,1,1,1,1]	1.183	[1,0,1,0,1,0,0,1,1,1]	1.755
7			[1,0,1,0,0,1,1,1,1,1]	1.511
8			[1,1,0,1,1,1,1,1,0,1]	1.508
9			[1,1,0,1,1,1,1,1,1,1]	1.511
10			[1,1,1,1,1,1,1,1,1,1]	1.491

https://doi.org/10.1371/journal.pone.0331741.t003

Table 4. Optimal RFD Parameter Values for Configuration in the 6-Story Frame.

Story	Total Number of RFDs					
	1	**2**	**3**	**4**	**5**	**6**
6	2711[a]	1801	1,253	796	2,781	824
	7.26[b]	15.49	16.72	17.55	22.21	11.61
5	–	2018	–	1986	2,540	1,774
		10.74		14.18	14.93	17.28
4	–	–	1,515	2,327	1,639	1,546
			17.14	17.02	21.43	10.50
3	–	–	–	–	2,662	1813
					14.26	20.35
2	–	–	–	–	–	2,719
						9.36
1	–	–	1,598	2,744	1990	2,840
			12.35	17.61	8.92	10.39

a: M_f (Kips.in), b: h_a (in).

https://doi.org/10.1371/journal.pone.0331741.t004

Furthermore, a similar trend is observed in the case of the 10-story structure, wherein the number of RFDs is altered from 7 to 10. Additionally, the optimal parameters for dampers pertaining to both the 6-story and 10-story frames are presented in Tables 4 and 5, respectively.

In Table 6, one can observe a comprehensive illustration of the distinctive characteristics pertaining to the maximum input energy, the hysteretic energy, as well as the dissipated energy, which are all meticulously delineated for the structural framework that incorporates the optimally designed RFDs, and this detailed analysis is subsequently juxtaposed with the corresponding energy characteristics of the structural framework that does not integrate such RFDs, specifically focusing on a 6-story frame.

It is clear from Table 6 that enhancing the number of dampers leads to a reduction in input energy, while the energy dissipated by the RFDs shows an upward trend. The results further clarify that optimizing the position and characteristics of the RFDs significantly diminishes the total hysteretic energy, thus mitigating seismic damage to the structure. The ideal results highlighted in Table 6 indicate that a substantial portion of the input energy is absorbed by the optimal RFDs, allowing for only a tiny fraction of the seismic input energy to be transferred to the structural components, ultimately resulting

Table 5. The optimal RFD parameter values for the allocation of RFDs in a 10-story frame.

Story	Total Number of RFDs									
	1	2	3	4	5	6	7	8	9	10
10	3971[a]	3,010	3,105	2,111	2,458	2,456	3,109	3,119	2,840	3,502
	8.23[b]	19.99	14.93	17.84	23.54	15.28	12.41	14.49	21.81	14.33
9		2,981				3,866	1,547		3,664	3,616
		16.41				11.98	14.44		23.41	11.93
8					2,147	2,159	3,547	3,857	3,311	2,715
					18.47	10.74	24.25	13.19	18.22	18.10
7			2,320				2,247	3,002	2,658	2,451
			18.74				18.11	7.37	19.18	13.63
6				1,159	1843		1,588	1815	484	1927
				16.41	15.29		17.58	19.81	6.92	18.82
5						2,921		2,120	2,525	2,256
						14.17		19.84	19.50	22.24
4				1,258	3,540			3,098	1,725	1,451
				16.32	22.31			17.56	21.09	11.24
3						2,451	1935			3,147
						17.13	21.02			13.13
2								1986	3,216	1,181
								18.31	17.48	14.36
1			1816	2,763	841	2,525	1984	2,471	2,432	3,221
			20.55	11.15	7.32	12.84	13.27	17.75	12.36	20.08

a: M_f (Kips.in), b: h_a (in).

https://doi.org/10.1371/journal.pone.0331741.t005

Table 6. Comparative analysis of maximum input, hysteretic, and dissipated energy in a 6-Story SMRF with various optimal RFD configurations.

Energy	Total Number of RFDs						
	0	1	2	3	4	5	6
E_i (Kips.in)	24,764	24,357 (1.64)*	24,003 (3.07)	23,519 (5.03)	22,143 (10.58)	21,408 (13.55)	21,312 (13.94)
E_{RFDs} (Kips.in)	–	11,148	12,295	13,821	15,754	17,925	18,012
E_h (Kips.in)	13,276	4,639 (65.06)*	3,237 (75.62)	2,218 (83.29)	1,271 (90.43)	238 (98.21)	199 (98.50)

* The percentage of reduction

https://doi.org/10.1371/journal.pone.0331741.t006

in less structural damage during seismic events. As shown in Table 6, increasing the number of RFDs from 5 to 6 corresponds to a reduction percentage in cumulative hysteretic energy of 98.21% and 98.50%, respectively. This pattern is also observed in input energy, with reduction percentages for the SMRF equipped with 5 and 6 RFDs documented at 13.5% and 13.94%, respectively. The dissipated energy values for the optimal configurations of 5 and 6 RFDs are recorded as 17,925 and 18,012 Kips.in, respectively. As a result, the significant change in dissipated energy when increasing the number of RFDs from 5 to 6 is not apparent. Therefore, the optimal number of dampers can be considered to be 5, and any further increase in the number of dampers may lead to substantial costs without providing a notable decrease in the structural seismic responses. Fig 16 displays the comparative evaluation of input, hysteretic, and dissipated energies during the simulated earthquake for the SMRF without RFDs compared to the SMRF fitted with the optimal RFDs.

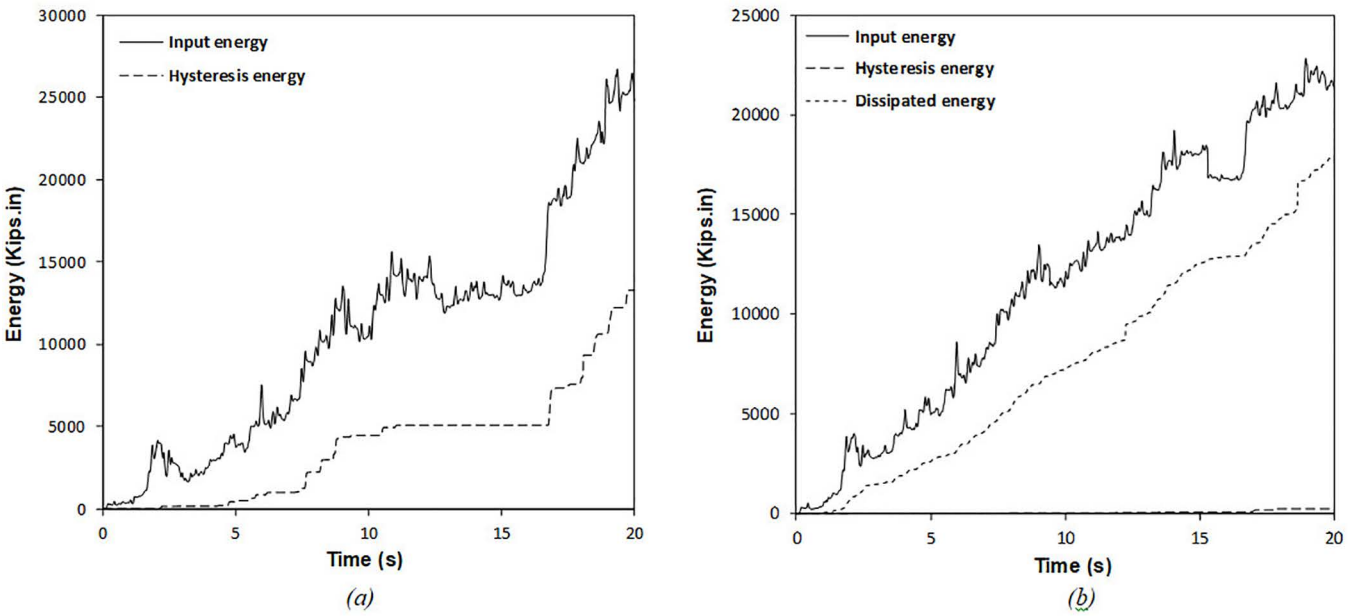


Fig 16. Energy time histories for the 6-story frame subjected to synthetic ground motion: (a) SMRF without RFDs and (b) SMRF with optimally configured RFDs.

https://doi.org/10.1371/journal.pone.0331741.g016

The findings indicate that the hysteretic energy of the SMRF, when integrated with the optimal RFDs, is substantially reduced during the simulated seismic event. Consequently, the structural integrity is preserved against significant structural damage. Fig 17 presents a comparative analysis of the hysteretic energy dissipation at the plastic hinges of the structure outfitted with five optimal dampers in contrast to that of the structure devoid of RFDs. It is evident that a significant proportion of the structural components within the system equipped with the five optimal dampers remains within the elastic limits, thus protecting the structural frame from severe damage.

Furthermore, Fig 18 illustrates the maximum story drift ratio for the 6-story SMRF both in the absence of RFDs and when equipped with the five optimized RFDs. As evident from the so-called figure, the incorporation of RFDs significantly reduces the inter-story drift ratio, demonstrating their effective performance. However, in the upper stories, the inter-story drift ratio of the frame with RFDs exceeds that of the frame without RFDs. This discrepancy arises because the optimization process is primarily energy-based, leading to a trade-off in drift reduction at higher levels.

Table 7 meticulously delineates the maximum input energy, the hysteretic energy, and the dissipated energy associated with the structural system that is equipped with the optimally designed and strategically placed RFDs, while simultaneously providing a comparative analysis with the corresponding energy metrics of the 10-story structural frame.
As demonstrated in Table 7, an increase in the number of dampers results in a reduction of the input energy, while the energy dissipated in experiments involving the RFDs shows a progressive increase. The results further clarify that the deliberate optimization of the placement and characteristics of the RFDs significantly diminishes the total hysteretic energy, thus aiding in the reduction of seismic damage to the structure. The optimal results presented in Table 7 indicate that a considerable proportion of the input energy is absorbed by the strategically positioned RFDs, while only a small fraction of the seismic input energy is transmitted to the structural elements, which subsequently lessens the structural damage incurred during seismic activity. From Table 7, it is observable that increasing the number of RFDs from 7 to 10 results in a reduction in cumulative hysteretic energy of 99.97% and 100%, respectively. This pattern is similarly noted in the input energy, with the reduction percentages for the SMRF outfitted with 7 and 10 RFDs recorded at 23.16% and

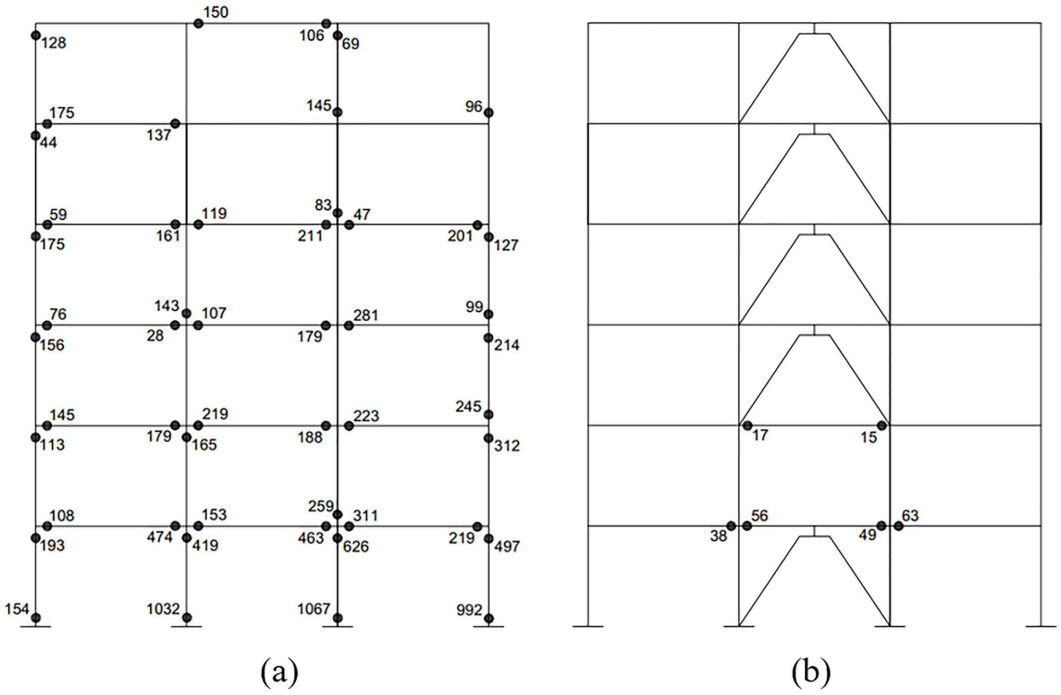


Fig 17. Comparison of hysteretic energy dissipation at each plastic hinge of the 6-story frame (a) without RFD (b) with optimal RFDs (unit: Kips.in).

https://doi.org/10.1371/journal.pone.0331741.g017

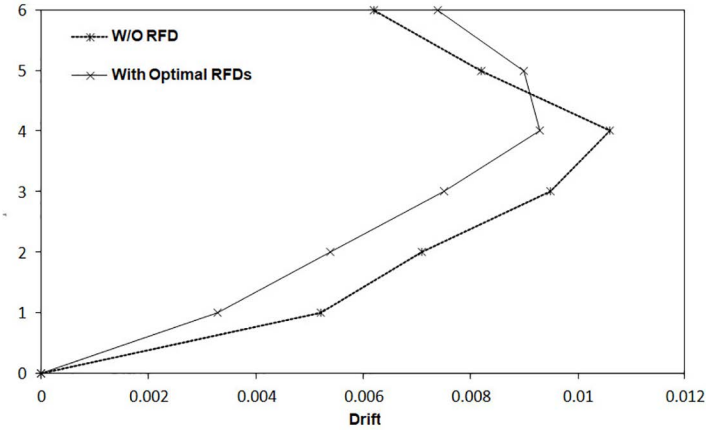


Fig 18. Comparative assessment of maximum structural drift with and without optimally designed RFDs.

https://doi.org/10.1371/journal.pone.0331741.g018

24.76%, respectively. The dissipated energy values for the optimal configurations of 7 and 10 RFDs are quantified as 7,331 and 7,409 Kips.in, respectively. Thus, the significant alteration in dissipated energy upon increasing the RFDs from 7 to 10 is negligible. Therefore, the optimal count of dampers may be regarded as 7, as any further augmentation in the number of dampers incurs significant construction costs without providing a meaningful reduction in structural seismic responses. Fig 19 presents a comparative analysis of the input, hysteretic, and dissipated energies during the artificially simulated earthquake for the SMRF devoid of RFDs and the optimally equipped RFDs-SMRF.

Table 7. Comparative evaluation of maximum input, hysteretic, and dissipated energy values in a 10-story SMRF with various optimally configured RFDs.

Energy	Total Number of RFDs										
	0	1	2	3	4	5	6	7	8	9	10
E_i (Kips.in)	14,413	14,073 (2.36)*	13,755 (4.57)	13,208 (8.36)	12,419 (13.83)	11,962 (17.01)	11,341 (21.31)	11,075 (23.16)	10,940 (24.10)	11,121 (22.84)	11,048 (24.76)
E_{RFDs} (Kips.in)	---	2,952	3,588	4,413	5,141	5,827	6,463	7,331	7,254	7,359	7,409
E_h (Kips.in)	3,542	3,283 (7.31)*	2,837 (19.90)	2,318 (34.56)	1,475 (58.36)	717 (79.76)	143 (95.96)	8 (99.77)	1 (99.97)	0 (100)	0 (100)

* The percentage of reduction

https://doi.org/10.1371/journal.pone.0331741.t007

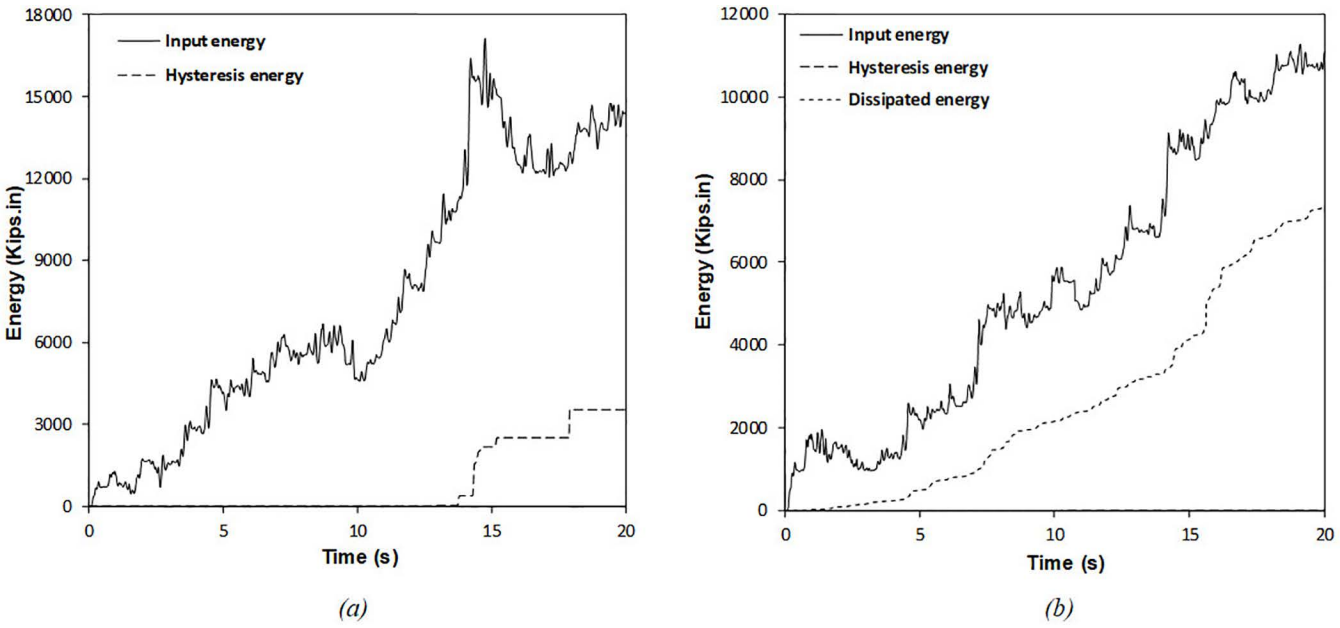


Fig 19. Time history of energy components in the 10-story frame subjected to the artificial record: (a) SMRF without RFD and (b) SMRF equipped with optimal RFDs.

https://doi.org/10.1371/journal.pone.0331741.g019

The findings indicate that the hysteretic energy of the SMRF outfitted with the optimal RFDs is substantially reduced during the simulated seismic event. Consequently, this structural configuration can be safeguarded against significant structural damages. Fig 20 presents a comparison of the hysteretic energy dissipation at the plastic hinges of the structure fitted with 7 optimal dampers against that of the structure lacking RFDs. It is noted that a considerable proportion of the structural components in the configuration with the 7 optimal dampers remain within the elastic limits, thereby shielding the frame from severe damage.

Moreover, Fig 21 delineates the maximum inter-story drift ratio for the 10-story SMRF both without RFDs and with the 7 optimized RFDs. The figure clearly demonstrates that the integration of RFDs leads to a marked reduction in the inter-story drift ratio, underscoring their efficacy. However, in the upper stories, particularly story number 9, the inter-story drift ratio of the frame with RFDs exceeds that of the frame without RFDs. This variance is attributable to the fact that the optimization process is predominantly energy-focused, resulting in a compromise in drift reduction at elevated levels.

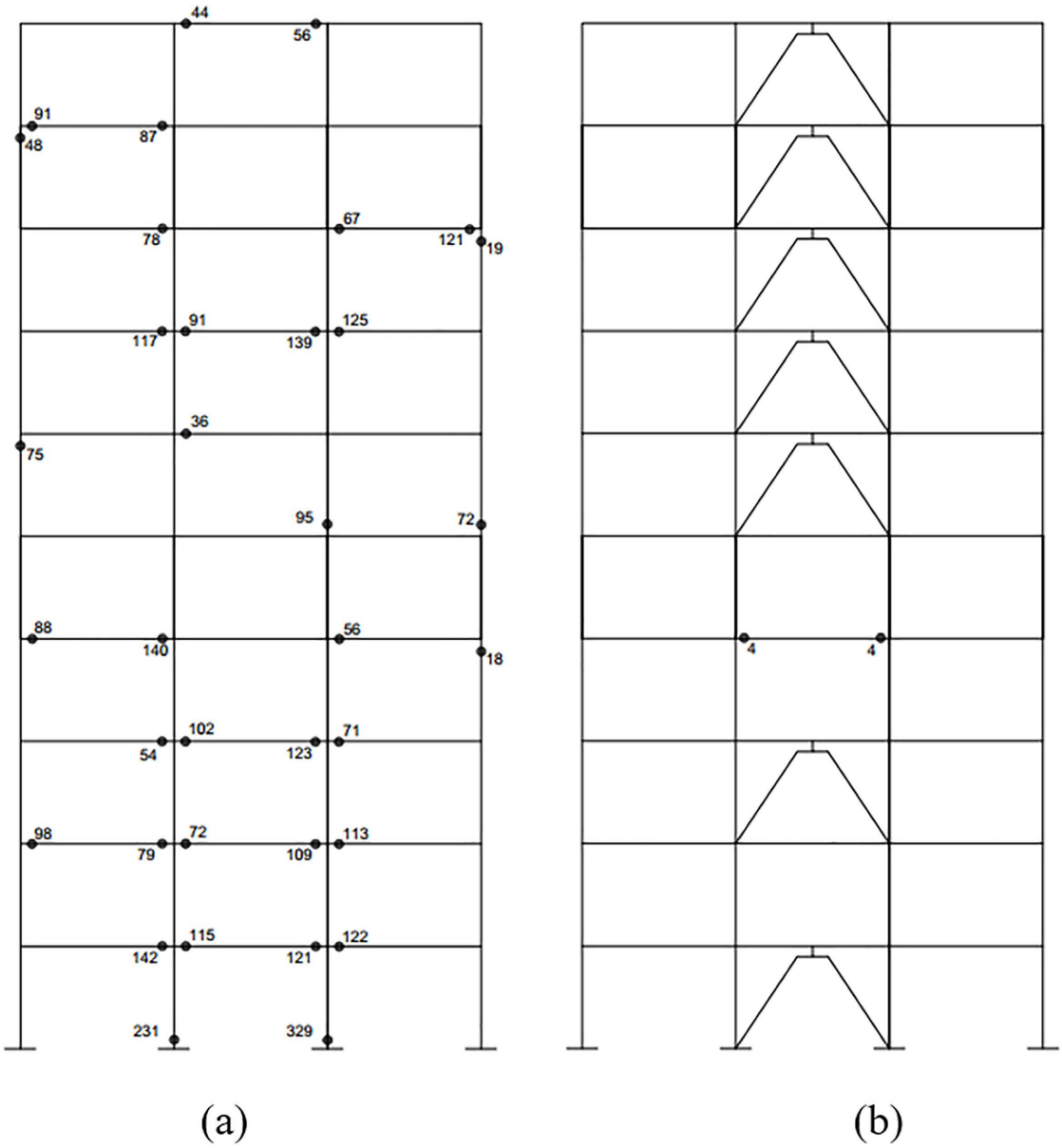


Fig 20. Comparison of hysteretic energy dissipation at each plastic hinge of the 10-story frame (a) without RFD (b) with optimal RFDs (unit: Kips.in).

https://doi.org/10.1371/journal.pone.0331741.g020

9. Conclusions

This research introduces a robust and comprehensive optimization strategy for the efficient design and strategic placement of rotational friction dampers (RFDs) within special moment-resisting frames (SMRFs), aiming to enhance their seismic performance. Leveraging a hybrid binary–real-coded particle swarm optimization (BRPSO) algorithm in conjunction with a seismic energy-based objective function, the study successfully identifies optimal damper configurations that significantly improve energy dissipation capacity while concurrently minimizing structural damage and inter-story drift. Through detailed sensitivity analyses, the study confirms that key RFD parameters—specifically the frictional moment (M_f) and the

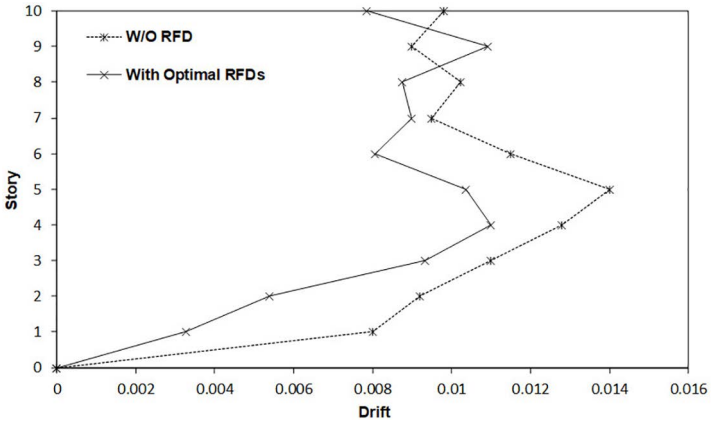


Fig 21. Comparative assessment of maximum structural drift with and without optimally designed RFDs.

https://doi.org/10.1371/journal.pone.0331741.g021

length of the rigid beam (h_a), have a profound impact on the dampers' capacity to attenuate seismic responses. These parameters emerge as critical design variables in optimizing the seismic performance of SMRFs. Furthermore, by incorporating the effects of soil-structure interaction (SSI), the research highlights the necessity of accounting for foundation flexibility and ground conditions, which substantially influence overall structural response and energy dissipation behavior during seismic events. Importantly, the findings reveal that simply increasing the number of dampers does not linearly enhance seismic performance. Beyond an optimal threshold, additional dampers contribute minimally to further reductions in structural demand. This underscores the importance of precise, performance-based damper allocation, as opposed to uniform or excessive deployment, thereby supporting both economic efficiency and structural effectiveness. Comparative performance assessments demonstrate that the optimized SMRFs achieve marked reductions in both hysteretic energy demands and residual deformations, reflecting notable improvements in structural stability across various earthquake scenarios. These improvements affirm the efficacy of the proposed optimization framework as a practical and scalable solution for the development of high-performance seismic protection systems. Ultimately, the presented methodology offers valuable insights for the design of cost-effective, resilient structural systems in mid- to high-rise buildings situated in seismically active regions.

Author contributions

Conceptualization: Hossein Jarrahi, Mohsen Khatibinia.

Data curation: Hossein Jarrahi.

Formal analysis: Hossein Jarrahi.

Investigation: Hossein Jarrahi, Mohsen Khatibinia.

Methodology: Mohsen Khatibinia.

Project administration: Hossein Jarrahi.

Software: Hossein Jarrahi, S.Javad Vaziri, Mohsen Khatibinia.

Supervision: Mohsen Khatibinia.

Visualization: S.Javad Vaziri.

Writing – original draft: S.Javad Vaziri.

Writing – review & editing: Mohsen Khatibinia.

References

1. Kulaksizoglu AA, Yalcin C, Yilmaz C. Analytical and experimental investigation of a motion amplified rotational friction damper. Engineering Structures. 2023;288:116184. https://doi.org/10.1016/j.engstruct.2023.116184
2. Rayegani A, Soureshjani OK, Alaee SAM, Mualla IH, Nemati F. Seismic Performance of Buildings Equipped with Four-Joint Rotational Friction Dampers in Mainshock–Aftershock Sequences. J Struct Eng. 2024;150(3). https://doi.org/10.1061/jsendh.steng-12980
3. Vaziri SJ, Rajabnejad H, Soleymani A. Ground motion parameters and damage correlation in plan irregular L-shape steel structure with BRB. Soil Dynamics and Earthquake Engineering. 2024;186:108916. https://doi.org/10.1016/j.soildyn.2024.108916
4. Xu G, Guo T. Advances in AI-powered civil engineering throughout the entire lifecycle. Adv Struct Eng. 2025;28(9):1515–41. https://doi.org/10.1177/13694332241307721
5. Javidan MM, Kim J. A rotational friction damper-brace for seismic design of resilient framed structures. Journal of Building Engineering. 2022;51:104248. https://doi.org/10.1016/j.jobe.2022.104248
6. Li D, Zhou Y. A force-resisting rotary friction damper (RFD): Verification and comparison with traditional RFD. Engineering Structures. 2022;273:115015. https://doi.org/10.1016/j.engstruct.2022.115015
7. Li J, Wang W, Kusunoki K, Maida Y, Wang Z. A simplified analysis method for estimating the peak responses of recentering structures with viscous damping systems. Earthq Engng Struct Dyn. 2024;53(1):472–95. https://doi.org/10.1002/eqe.4033
8. Noureldin M, Memon SA, Gharagoz M, Kim J. Performance-based seismic retrofit of RC structures using concentric braced frames equipped with friction dampers and disc springs. Engineering Structures. 2021;243:112555. https://doi.org/10.1016/j.engstruct.2021.112555
9. Shirkhani A, Farahmand Azar B, Charkhtab Basim M. Seismic loss assessment of steel structures equipped with rotational friction dampers subjected to intensifying dynamic excitations. Engineering Structures. 2021;238:112233. https://doi.org/10.1016/j.engstruct.2021.112233
10. Araz O. Optimum three-element tuned mass damper for damped main structures under ground acceleration. El-Cezeri. 2021;8(3):1264–71.
11. Araz O, Kahya V. Optimization of non-traditional tuned mass damper for damped structures under harmonic excitation. Uludağ Üniversitesi Mühendislik Fakültesi Dergisi. 2021;26(3):1021–34.
12. Fahimi Farzam M, Hojat Jalali H. Tandem tuned mass damper inerter for passive control of buildings under seismic loads. Structural Contr & Hlth. 2022;29(9). https://doi.org/10.1002/stc.2987
13. Kahya V, Araz O. Series multiple tuned mass dampers for vibration control of highspeed railway bridges. Insights and innovations in structural engineering, Mechanics and computation. CRC Press. 2016. p. 143–8.
14. Kahya V, Araz O. A sequential approach based design of multiple tuned mass dampers under harmonic excitation. Sigma Journal of Engineering and Natural Sciences. 2019;37(1):225–39.
15. Pisal AY, Jangid RS. Vibration control of bridge subjected to multi-axle vehicle using multiple tuned mass friction dampers. Int J Adv Struct Eng. 2016;8(2):213–27. https://doi.org/10.1007/s40091-016-0124-y
16. Aiken ID. Earthquake simulator testing and analytical studies of two energy-absorbing systems for multistory structures. Berkeley: University of California. 1990.
17. Constantinou MC, Reinhorn AM, Mokha A, Watson R. Displacement Control Device for Base-Isolated Bridges. Earthquake Spectra. 1991;7(2):179–200. https://doi.org/10.1193/1.1585625
18. Filiatrault A, Cherry S. Parameters influencing the design of friction damped structures. Can J Civ Eng. 1989;16(5):753–66. https://doi.org/10.1139/l89-110
19. Filiatrault A, Cherry S. Seismic Design Spectra for Friction-Damped Structures. J Struct Eng. 1990;116(5):1334–55. https://doi.org/10.1061/(asce)0733-9445(1990)116:5(1334)
20. Fu Y, Cherry S. Simplified seismic code design procedure for friction-damped steel frames. Can J Civ Eng. 1999;26(1):55–71. https://doi.org/10.1139/l98-043
21. Grigorian CE, Yang TS, Popov EP. Slotted Bolted Connection Energy Dissipators. Earthquake Spectra. 1993;9(3):491–504. https://doi.org/10.1193/1.1585726
22. Nims DK, Richter PJ, Bachman RE. The Use of the Energy Dissipating Restraint for Seismic Hazard Mitigation. Earthquake Spectra. 1993;9(3):467–89. https://doi.org/10.1193/1.1585725
23. Colajanni P, Papia M. Hysteretic Behavior Characterization of Friction-Damped Braced Frames. J Struct Eng. 1997;123(8):1020–8. https://doi.org/10.1061/(asce)0733-9445(1997)123:8(1020)
24. Pall AS, Marsh C. Response of Friction Damped Braced Frames. J Struct Div. 1982;108(6):1313–23. https://doi.org/10.1061/jsdeag.0005968
25. FitzGerald TF, Anagnos T, Goodson M, Zsutty T. Slotted Bolted Connections in Aseismic Design for Concentrically Braced Connections. Earthquake Spectra. 1989;5(2):383–91. https://doi.org/10.1193/1.1585528
26. Askari M, Li J, Samali B. Semi-Active LQG Control of Seismically Excited Nonlinear Buildings using Optimal Takagi-Sugeno Inverse Model of MR Dampers. Procedia Engineering. 2011;14:2765–72. https://doi.org/10.1016/j.proeng.2011.07.348
27. Brando G, D'Agostino F, De Matteis G. Experimental tests of a new hysteretic damper made of buckling inhibited shear panels. Mater Struct. 2013;46(12):2121–33. https://doi.org/10.1617/s11527-013-0040-6

28. Brando G, D'Agostino F, De Matteis G. Seismic performance of MR frames protected by viscous or hysteretic dampers. Struct Design Tall Spec Build. 2015;24(9):653–71. https://doi.org/10.1002/tal.1204
29. Brando G, De Matteis G. Design of low strength-high hardening metal multi-stiffened shear plates. Engineering Structures. 2014;60:2–10. https://doi.org/10.1016/j.engstruct.2013.12.005
30. Chan RWK, Albermani F, Kitipornchai S. Experimental study of perforated yielding shear panel device for passive energy dissipation. Journal of Constructional Steel Research. 2013;91:14–25. https://doi.org/10.1016/j.jcsr.2013.08.013
31. De Matteis G, Sarracco G, Brando G. Experimental tests and optimization rules for steel perforated shear panels. Journal of Constructional Steel Research. 2016;123:41–52. https://doi.org/10.1016/j.jcsr.2016.04.025
32. Levy R, Lavan O. Fully stressed design of passive controllers in framed structures for seismic loadings. Struct Multidisc Optim. 2006;32(6):485–98. https://doi.org/10.1007/s00158-005-0558-5
33. Saeedi F, Shabakhty N, Mousavi SR. Seismic assessment of steel frames with triangular-plate added damping and stiffness devices. Journal of Constructional Steel Research. 2016;125:15–25. https://doi.org/10.1016/j.jcsr.2016.06.011
34. Mualla IH, Belev B. Performance of steel frames with a new friction damper device under earthquake excitation. Engineering Structures. 2002;24(3):365–71. https://doi.org/10.1016/s0141-0296(01)00102-x
35. Patel CC, Jangid RS. Dynamic response of adjacent structuresconnected by friction damper. Earthquakes and Structures. 2011;2(2):149–69. https://doi.org/10.12989/EAS.2011.2.2.149
36. Kim J, Choi H, Min K. Use of rotational friction dampers to enhance seismic and progressive collapse resisting capacity of structures. Structural Design Tall Build. 2011;20(4):515–37. https://doi.org/10.1002/tal.563
37. Kaur N, Matsagar VA, Nagpal AK. Earthquake response of mid-rise to high-rise buildings with friction dampers. International Journal of High-Rise Buildings. 2012;1(4):311–32.
38. Choi KS, Kim HJ. Strength demand of hysteretic energy dissipating devices alternative to coupling beams in high-rise buildings. International Journal of High-Rise Buildings. 2014;3(2):107–20.
39. Sanati M, Khadem SE, Mirzabagheri S, Sanati H, Khosravieh MY. Performance evaluation of a novel rotational damper for structural reinforcement steel frames subjected to lateral excitations. Earthq Eng Eng Vib. 2014;13(1):75–84. https://doi.org/10.1007/s11803-014-0213-5
40. Mirzabagheri S, Sanati M, Aghakouchak AA, Khadem SE. Experimental and numerical investigation of rotational friction dampers with multi units in steel frames subjected to lateral excitation. Archives of Civil and Mechanical Engineering. 2015;15(2):479–91. https://doi.org/10.1016/j.acme.2014.05.009
41. Bonchev G, Belev B, Mualla I. 11.32: Linked columns with friction dampers as a technique for seismic retrofit of steel moment resisting frames. ce papers. 2017;1(2–3):3092–9. https://doi.org/10.1002/cepa.361
42. Anoushehei M, Daneshjoo F, Mahboubi S, Hashemi MH. Empirical Evaluation of Cyclic Behavior of Rotational Friction Dampers with Different Metal Pads. Scientia Iranica. 2018;25(6):3021–9. https://doi.org/10.24200/sci.2017.4225
43. Nabid N, Hajirasouliha I, Petkovski M. A Practical Method for Optimum Seismic Design of Friction Wall Dampers. Earthquake Spectra. 2017;33(3):1033–52. https://doi.org/10.1193/110316eqs190m
44. Nabid N, Hajirasouliha I, Petkovski M. Performance-based optimisation of RC frames with friction wall dampers using a low-cost optimisation method. Bull Earthquake Eng. 2018;16(10):5017–40. https://doi.org/10.1007/s10518-018-0380-2
45. Apostolakis G, Dargush GF. Optimal seismic design of moment-resisting steel frames with hysteretic passive devices. Earthq Engng Struct Dyn. 2010;39(4):355–76. https://doi.org/10.1002/eqe.944
46. Takewaki I. Optimal damper placement for minimum transfer functions. Earthquake Engng Struct Dyn. 1997;26(11):1113–24. https://doi.org/10.1002/(sici)1096-9845(199711)26:11<1113::aid-eqe696>3.0.co;2-x
47. Zhang R, Soong TT. Seismic Design of Viscoelastic Dampers for Structural Applications. J Struct Eng. 1992;118(5):1375–92. https://doi.org/10.1061/(asce)0733-9445(1992)118:5(1375)
48. Shukla AK, Datta TK. Optimal use of viscoelastic dampers in building frames for seismic force. J Struct Eng. 1999;125(4):401– 9. https://doi.org/10.1061/(ASCE)0733-9445(1999)125:4(401). 2-s2.0-0033114899.
49. Moreschi LM, Singh MP. Design of yielding metallic and friction dampers for optimal seismic performance. Earthq Engng Struct Dyn. 2003;32(8):1291–311. https://doi.org/10.1002/eqe.275
50. Fallah N, Honarparast S. NSGA-II based multi-objective optimization in design of Pall friction dampers. Journal of Constructional Steel Research. 2013;89:75–85. https://doi.org/10.1016/j.jcsr.2013.06.008
51. Miguel LFF, Miguel LFF, Lopez RH. Simultaneous optimization of force and placement of friction dampers under seismic loading. Engineering Optimization. 2016;48(4):582–602. https://doi.org/10.1080/0305215x.2015.1025774
52. Kim J, An S. Optimal distribution of friction dampers for seismic retrofit of a reinforced concrete moment frame. Advances in Structural Engineering. 2016;20(10):1523–39. https://doi.org/10.1177/1369433216683197
53. Xu G, Guo T, Li A, Zhou T, Shuang C. Seismic Performance of Steel Frame Structures with Novel Self-Centering Beams: Shaking-Table Tests and Numerical Analysis. J Struct Eng. 2025;151(3). https://doi.org/10.1061/jsendh.steng-13516

54. Xu G, Guo T, Li A. Self-Centering Rotational Joints for Seismic Resilient Steel Moment Resisting Frame. J Struct Eng. 2023;149(2). https://doi.org/10.1061/jsendh.steng-11475
55. Xu G, Guo T, Li A, Wu Y, Zhang H, Zhi G. Innovative self-centering tension-only braces for enhanced seismic resilience in frame structures: An experimental and numerical analysis. Eng Struct. 2024;319:118816. https://doi.org/10.1016/j.engstruct.2024.118816
56. Jarrahi H, Asadi A, Khatibinia M, Etedali S. Optimal design of rotational friction dampers for improving seismic performance of inelastic structures. Journal of Building Engineering. 2020;27:100960. https://doi.org/10.1016/j.jobe.2019.100960
57. Jarrahi H, Asadi A, Khatibinia M, Etedali S, Paknehad S. Soil-structure interaction effects on the seismic performance of steel moment-resisting frames equipped with optimal rotational friction dampers. Structures. 2022;43:449–64. https://doi.org/10.1016/j.istruc.2022.05.118
58. Kapasakalis KA. Seismic retrofit of multi-story structures with KDamper-based vibration control systems considering soil–structure-interaction. Soil Dynamics and Earthquake Engineering. 2025;196:109429. https://doi.org/10.1016/j.soildyn.2025.109429
59. Ozgan K, Kılıçer S, Daloglu AT. Soil–Structure Interaction Effect on the Resistance of a Steel Frame against Progressive Collapse Using Linear Static and Nonlinear Dynamic Procedures. J Perform Constr Facil. 2023;37(1). https://doi.org/10.1061/jpcfev.cfeng-4181
60. Khatibinia M, Gharehbaghi S, Moustafa A. Seismic Reliability-Based Design Optimization of Reinforced Concrete Structures Including Soil-Structure Interaction Effects. Earthquake Engineering - From Engineering Seismology to Optimal Seismic Design of Engineering Structures. InTech. 2015. https://doi.org/10.5772/59641
61. Wolf JP, Song C. Some cornerstones of dynamic soil–structure interaction. Engineering Structures. 2002;24(1):13–28. https://doi.org/10.1016/s0141-0296(01)00082-7
62. Vaziri SJ, Vahdani R, Souri O. Seismic evaluation of BRBF steel structures with L-shaped irregular plan considering soil-structure interaction. Bull Earthquake Eng. 2024. https://doi.org/10.1007/s10518-024-01963-4
63. Wegner JL, Yao MM, Zhang X. Dynamic wave–soil–structure interaction analysis in the time domain. Computers & Structures. 2005;83(27):2206–14. https://doi.org/10.1016/j.compstruc.2005.04.004
64. American Society of Civil Engineers ASCE. Minimum design loads and associated criteria for buildings and other structures. Reston (VA): American Society of Civil Engineers; 2017.
65. Bharti AK, Garg V, Chandrawanshi S. A critical review of seismic soil-structure interaction analysis. Structures. 2025;72:108221. https://doi.org/10.1016/j.istruc.2025.108221
66. Bapir B, Abrahamczyk L, Wichtmann T, Prada-Sarmiento LF. Soil-structure interaction: A state-of-the-art review of modeling techniques and studies on seismic response of building structures. Front Built Environ. 2023;9. https://doi.org/10.3389/fbuil.2023.1120351
67. Araz O, Elias S. Performance of differently arranged double-tuned mass dampers for structural seismic response control including soil-structure interaction. Engineering Structures. 2024;319:118841. https://doi.org/10.1016/j.engstruct.2024.118841
68. Araz O. Effect of basic parameters defining principal soil-structure interaction on seismic control of structures equipped with optimum tuned mass damper. Soil Dynam Earthquake Eng. 2025;189:109085. https://doi.org/10.1016/j.soildyn.2024.109085
69. Wu Y, Zhao M, Gao Z, Du X. Seismic performance analysis of structure equipped with tuned mass dampers considering nonlinear soil-structure interaction effects. Structures. 2024;63:106425. https://doi.org/10.1016/j.istruc.2024.106425
70. Behnamfar F, Banizadeh M. Effects of soil–structure interaction on distribution of seismic vulnerability in RC structures. Soil Dynamics and Earthquake Engineering. 2016;80:73–86. https://doi.org/10.1016/j.soildyn.2015.10.007
71. El Ganainy H, El Naggar MH. Seismic performance of three-dimensional frame structures with underground stories. Soil Dynamics and Earthquake Engineering. 2009;29(9):1249–61. https://doi.org/10.1016/j.soildyn.2009.02.003
72. Elias S, Djerouni S. Optimum tuned mass damper inerter under near-fault pulse-like ground motions of buildings including soil-structure interaction. Journal of Building Engineering. 2024;85:108674. https://doi.org/10.1016/j.jobe.2024.108674
73. Khatibinia M, Salajegheh E, Salajegheh J, Fadaee MJ. Reliability-based design optimization of reinforced concrete structures including soil–structure interaction using a discrete gravitational search algorithm and a proposed metamodel. Engineering Optimization. 2013;45(10):1147–65. https://doi.org/10.1080/0305215x.2012.725051
74. Wang L, Zhou Y, Zhou Z. Seismic response control of tall building using semi-active tuned mass damper considering soil-structure interaction. Soil Dynamics and Earthquake Engineering. 2024;187:108987. https://doi.org/10.1016/j.soildyn.2024.108987
75. Sadeghi A, Kazemi H, Hossein M, Razmkhah AS. Probabilistic investigation of the pounding effect in steel moment resisting frames with equal and unequal heights. 2024.
76. Sadeghi A, Kazemi H, Mehdizadeh K, Jadali F. Fragility analysis of steel moment-resisting frames subjected to impact actions. J Build Rehabil. 2022;7(1). https://doi.org/10.1007/s41024-022-00165-2
77. Sadeghi A, Kazemi H, Samadi M. Reliability and reliability-based sensitivity analyses of steel moment-resisting frame structure subjected to extreme actions. Fracture and Structural Integrity. 2021;15(57):138–59.
78. Nielsen LO, Mualla IH. A Friction Damping System Low Order Behavior and Design. Civil Engineering. 2002;1–15.
79. Mualla IH. Experimental & computational evaluation of a new friction damper device. Dept. of Structural Engineering and Materials, Technical. 2000.

80. F ZT, J HW. Earthquake energy absorption in SDOF structures. Journal of Structural Engineering. 1984;110(8):1757–72. https://doi.org/10.1061/(ASCE)0733-9445(1984)110:8(1757)
81. Filiatrault A, Léger P, Tinawi R. On the computation of seismic energy in inelastic structures. Engineering Structures. 1994;16(6):425–36. https://doi.org/10.1016/0141-0296(94)90057-4
82. M. TJ, M. NJ. Inelastic modeling and seismic energy dissipation. Journal of Structural Engineering. 1987;113(6):1373–7. https://doi.org/10.1061/(ASCE)0733-9445(1987)113:6(1373)
83. Léger P, Dussault S. Seismic-Energy Dissipation in MDOF Structures. J Struct Eng. 1992;118(5):1251–69. https://doi.org/10.1061/(asce)0733-9445(1992)118:5(1251)
84. Uang C, Bertero VV. Evaluation of seismic energy in structures. Earthq Engng Struct Dyn. 1990;19(1):77–90. https://doi.org/10.1002/eqe.4290190108
85. Jarrahi H, Asadi A, Khatibinia M, Etedali S, Samadi A. Simultaneous optimization of placement and parameters of rotational friction dampers for seismic-excited steel moment-resisting frames. Soil Dynamics and Earthquake Engineering. 2020;136:106193. https://doi.org/10.1016/j.soildyn.2020.106193
86. Etedali S, Akbari M, Seifi M. MOCS-based optimum design of TMD and FTMD for tall buildings under near-field earthquakes including SSI effects. Soil Dynamics and Earthquake Engineering. 2019;119:36–50. https://doi.org/10.1016/j.soildyn.2018.12.027
87. Gharehbaghi S, Khatibinia M. Optimal seismic design of reinforced concrete structures under time-history earthquake loads using an intelligent hybrid algorithm. Earthq Eng Eng Vib. 2015;14(1):97–109. https://doi.org/10.1007/s11803-015-0009-2
88. Keshtegar B, Etedali S. Nonlinear mathematical modeling and optimum design of tuned mass dampers using adaptive dynamic harmony search algorithm. Struct Control Health Monit. 2018;25(7):e2163. https://doi.org/10.1002/stc.2163
89. Sadeghi A, Kazemi H, Samadi M. Single and multi-objective optimization of steel moment-resisting frame buildings under vehicle impact using evolutionary algorithms. J Build Rehabil. 2021;6(1). https://doi.org/10.1007/s41024-021-00117-2
90. Shahi M, Sohrabi MR, Etedali S. Seismic Control of High-Rise Buildings Equipped with ATMD Including Soil-Structure Interaction Effects. J Earthquake and Tsunami. 2018;12(03):1850010. https://doi.org/10.1142/s1793431118500100
91. Shayesteh Bilondi MR, Yazdani H, Khatibinia M. Seismic energy dissipation-based optimum design of tuned mass dampers. Struct Multidisc Optim. 2018;58(6):2517–31. https://doi.org/10.1007/s00158-018-2033-0
92. Shobeiri V. The optimal design of structures using ACO and EFG. Engineering with Computers. 2016;32(4):645–53. https://doi.org/10.1007/s00366-016-0443-4
93. Shobeiri V, Nasirai C. (2012). A hybrid ant colony and genetic algorithm for topology optimization of two-dimensional continuous environments. Majl J Mechatron Syst, 1(2), 18–24.
94. Tsiptsis IN, Liimatainen L, Kotnik T, Niiranen J. Structural optimization employing isogeometric tools in Particle Swarm Optimizer. Journal of Building Engineering. 2019;24:100761. https://doi.org/10.1016/j.jobe.2019.100761
95. Zamani A-A, Tavakoli S, Etedali S, Sadeghi J. Online tuning of fractional order fuzzy PID controller in smart seismic isolated structures. Bull Earthquake Eng. 2017;16(7):3153–70. https://doi.org/10.1007/s10518-017-0294-4
96. Khatibinia M, Shokri MA, Jarrahi H. Optimal design of chevron braced friction damper for mainshock–aftershock vulnerability control. Journal of Constructional Steel Research. 2024;218:108739. https://doi.org/10.1016/j.jcsr.2024.108739
97. Wong KK. Seismic energy dissipation of inelastic structures with tuned mass dampers. J Eng Mech. 2008;134(2):163–72. https://doi.org/10.1061/(ASCE)0733-9399(2008)134:2(163)
98. Wong KK, Johnson J. Seismic Energy Dissipation of Inelastic Structures with Multiple Tuned Mass Dampers. J Eng Mech. 2009;135(4):265–75. https://doi.org/10.1061/(asce)0733-9399(2009)135:4(265)
99. K. WK. Seismic energy dissipation of inelastic structures with tuned mass dampers. Journal of Engineering Mechanics. 2008;134(2):163–72. https://doi.org/10.1061/(ASCE)0733-9399(2008)134:2(163)
100. Ibarra LF, Medina RA, Krawinkler H. Hysteretic models that incorporate strength and stiffness deterioration. Earthquake Engng Struct Dyn. 2005;34(12):1489–511. https://doi.org/10.1002/eqe.495
101. Lignos DG, Krawinkler H. Deterioration Modeling of Steel Components in Support of Collapse Prediction of Steel Moment Frames under Earthquake Loading. J Struct Eng. 2011;137(11):1291–302. https://doi.org/10.1061/(asce)st.1943-541x.0000376
102. Araz O. Effect of PGV/PGA ratio on seismic-induced vibrations of structures equipped with parallel tuned mass dampers considering SSI. Structures. 2024;68:107188. https://doi.org/10.1016/j.istruc.2024.107188
103. Jaya KP, Meher Prasad A. Embedded foundation in layered soil under dynamic excitations. Soil Dynamics and Earthquake Engineering. 2002;22(6):485–98. https://doi.org/10.1016/s0267-7261(02)00032-5
104. Rayhani MH, El Naggar MH. Numerical Modeling of Seismic Response of Rigid Foundation on Soft Soil. Int J Geomech. 2008;8(6):336–46. https://doi.org/10.1061/(asce)1532-3641(2008)8:6(336)
105. Zhang Y, Conte JP, Yang Z, Elgamal A, Bielak J, Acero G. Two-Dimensional Nonlinear Earthquake Response Analysis of a Bridge-Foundation-Ground System. Earthquake Spectra. 2008;24(2):343–86. https://doi.org/10.1193/1.2923925

106. Lysmer J, Kuhlemeyer RL. Finite dynamic model for infinite media. Journal of the Engineering Mechanics Division. 1969;95(4):859–77.

107. Coello Coello CA. Theoretical and numerical constraint-handling techniques used with evolutionary algorithms: a survey of the state of the art. Computer Methods in Applied Mechanics and Engineering. 2002;191(11–12):1245–87. https://doi.org/10.1016/s0045-7825(01)00323-1

108. Chen T-Y, Chen C-J. Improvements of simple genetic algorithm in structural design. Int J Numer Meth Engng. 1997;40(7):1323–34. https://doi.org/10.1002/(sici)1097-0207(19970415)40:7<1323::aid-nme117>3.0.co;2-t

109. Yazdani H, Khatibinia M, Gharehbaghi S, Hatami K. Probabilistic Performance-Based Optimum Seismic Design of RC Structures Considering Soil–Structure Interaction Effects. ASCE-ASME J Risk Uncertainty Eng Syst, Part A: Civ Eng. 2017;3(2). https://doi.org/10.1061/ajrua6.0000880

110. Khatibinia M, Yazdani H. Accelerated multi-gravitational search algorithm for size optimization of truss structures. Swarm and Evolutionary Computation. 2018;38:109–19. https://doi.org/10.1016/j.swevo.2017.07.001

111. Rajeev S, Krishnamoorthy CS. Discrete optimization of structures using genetic algorithms. J Struct Eng 1992;118(5):1233–50.

112. Wu J, Chen G, Lou M. Seismic effectiveness of tuned mass dampers considering soil-structure interaction. Earthquake Engng Struct Dyn. 1999;28(11):1219–33. https://doi.org/10.1002/(sici)1096-9845(199911)28:11<1219::aid-eqe861>3.0.co;2-g